AWARD NUMBER: W81XWH-14-1-0456

TITLE: Using Arrays of Microelectrodes Implanted in Residual Peripheral Nerves to Provide Dextrous Control of, and Modulated Sensory Feedback from, a Hand Prosthesis

PRINCIPAL INVESTIGATOR: Bradley Greger, PhD

CONTRACTING ORGANIZATION: Arizona State University
Tempe, AZ 85287

REPORT DATE: October 2017

TYPE OF REPORT: Annual

PREPARED FOR: U.S. Army Medical Research and Materiel Command
Fort Detrick, Maryland 21702-5012

REPORT DOCUMENTATION PAGE

Form Approved
OMB No. 0704-0188

1. REPORT DATE	**2. REPORT TYPE**	**3. DATES COVERED**
October 2017	Annual	30 Sep 2016 - 29 Sep 2017

4. TITLE AND SUBTITLE
Using Arrays of Microelectrodes Implanted in Residual Peripheral Nerves to Provide Dexterous Control of, and Modulated Sensory Feedback from, a Hand Prosthesis

5a. CONTRACT NUMBER

5b. GRANT NUMBER
W81XWH-14-1-0456

5c. PROGRAM ELEMENT NUMBER

6. AUTHOR(S)
Bradley Greger, PhD

Email: bradley.greger@asu.edu

5d. PROJECT NUMBER

5e. TASK NUMBER

5f. WORK UNIT NUMBER

7. PERFORMING ORGANIZATION NAME(S) AND ADDRESS(ES)
Arizona State University
Tempe, AZ 85287

8. PERFORMING ORGANIZATION REPORT NUMBER

9. SPONSORING / MONITORING AGENCY NAME(S) AND ADDRESS(ES)
U.S. Army Medical Research and Materiel Command
Fort Detrick, Maryland 21702-5012

10. SPONSOR/MONITOR'S ACRONYM(S)

11. SPONSOR/MONITOR'S REPORT NUMBER(S)

12. DISTRIBUTION / AVAILABILITY STATEMENT
Approved for Public Release; Distribution Unlimited

13. SUPPLEMENTARY NOTES

14. ABSTRACT
The proposed research is focused on restoration of hand motor and sensory functions by utilizing a direct electrical interface with residual peripheral nerves. The direct connection with the residual nerves will enable the patient to have intuitive control over and receive touch sensation from a prosthetic hand that are not provided by current forearm prostheses. The improvement in intuitive control and the providing of sensory feedback will allow patients to use highly articulate prosthetic hands with improved long-term functional outcomes for military personnel and civilians with a forearm amputation. Based on preliminary studies in peripheral nerves it is possible to decode finger movements from electrophysiological signals recorded from peripheral nerves, and to evoke somatosensory perceptions through micro-stimulation of peripheral nerves. The proposed research will determine the type and complexity of movements that can be controlled by a direction connection to arm nerves, and will also determine the type and range touch sensations that can be provide through a direct connection to residual nerves.

15. SUBJECT TERMS-

Nothing listed

16. SECURITY CLASSIFICATION OF:			**17. LIMITATION OF ABSTRACT**	**18. NUMBER OF PAGES**	**19a. NAME OF RESPONSIBLE PERSON**
					USAMRMC
a. REPORT	**b. ABSTRACT**	**c. THIS PAGE**			**19b. TELEPHONE NUMBER** *(include area code)*
U	U	U	UU	45	

Table of Contents

Page

1. **INTRODUCTION:** The proposed research is focused on restoration of hand motor and sensory functions by utilizing a direct electrical interface with residual peripheral nerves. The direct connection with the residual nerves will enable the patient to have intuitive control over and receive touch sensation from a prosthetic hand that are not provided by current forearm prostheses. The improvement in intuitive control and the providing of sensory feedback will allow patients to use highly articulate prosthetic hands with improved long-term functional outcomes for military personnel and civilians with a forearm amputation. Based on preliminary studies in peripheral nerves it is possible to decode finger movements from electrophysiological signals recorded from peripheral nerves, and to evoke somatosensory perceptions through micro-stimulation of peripheral nerves. The proposed research will determine the type and complexity of movements that can be controlled by a direction connection to arm nerves, and will also determine the type and range touch sensations that can be provide through a direct connection to residual nerves.

2. **KEYWORDS:** Peripheral Nerve Interface, Prosthetic Hand, Neural Prosthesis, Sensory Feedback, Micro-stimulation, Electrophysiology, Action Potentials, Micro-electrode, poly-Longitudinal Intrafascicular Electrode (poly-LIFE)

3. **ACCOMPLISHMENTS:** Provided in italics in appropriate sections.

   What were the major goals of the project?

   Specific Aim 1: Dexterous control of, and sensory feedback from, an advanced prosthetic hand will be provided using micro-electrode arrays implanted in residual peripheral nerves

   Major Goal 1: Preparation for Studies

   Subtask 1.1: Regulatory Approvals (Months 1 – 4)

   - Mayo Clinic: Dr. Shelley Noland and Nicole Cevette oversee writing and submission of protocol and associated documents for IRB and HRPO.
   - Dr. Greger will assist in writing and submission of IRB and HRPO documents.

     <u>100% complete.</u>
     - *Study protocol approved by Mayo Clinic IRB on 5-Aug-2016.*
     - *ASU IRB confirms Mayo Clinic as external IRB of record on 10-Aug-2016.*
     - *Mayo Clinic IRB, approved study protocol, 05-Aug-2016*
     - *ASU confirmed external IRB (Mayo Clinic), 10-Aug-2016*
     - *USAMRMC ORP HRPO approved this greater than minimal risk study for the screening of 12 subjects to accrue 6 subjects. Letter received 31-Oct-2017.*
     - *The Mayo Clinic Institutional Review Board (IRB) approved continuation of the protocol on 3 August 2017*
     - *USAMRMC ORP HRPO approved the continuing review report for this greater than minimal risk study for the screening of 12 subjects to accrue 6 subjects. This approval will expire on 2 August 2018. Letter received 01-Feb-2018.*

   Subtask 1.2: Micro-electrode Arrays. (Months 4 – 30)

- Production of 9 human-ready Sputtered Iridium-Oxide (SIROF) micro-electrode arrays consisting of 100 electrodes.

  50% complete.
  - Design and drawings of micro-electrode arrays complete and purchasing quotes obtained from Blackrock Microsystems.

- Measure impedances on all electrodes in each array prior to sterilization, and if possible after explantation at the end of the study.

  50% complete.
  - *Instrumentation to obtain impedances on micro-electrode arrays at multiple frequencies currently in place and validated.*

- Obtain light microscope images of the arrays prior to implantation and after explantation.

  30% complete.
  - *Contract in place to perform light and electron microscopy on the micro-electrode arrays with the Aberration Corrected Electron Microscopy core facility at ASU. Have obtained test images.*

Major Task 2: Implantation and explantation of micro-electrode arrays in a residual nerve of patients with trans-humeral, trans-radial, or elbow disarticulation amputations

Subtask 2.1: Patient Recruitment (Months 4 – 30)

- Volunteers will be recruited, and informed consent obtained at the Mayo Clinic using the procedure in the approved IRB protocol.
- We expect to recruit 6 patients (~2/year) for participation in the study.

  50% complete.
  - *Patient recruitment materials developed and approved.*
  - *Made presentation to surgeons at Arizona Center for Hand Surgery.*
  - *Contacted the 67 potential candidates identified by mail and phone.*
  - *Identified and qualified the first subject for participation in study*

Subtask 2.2: Micro-electrode array implantation (Months 4 – 30)

- Implantation of one micro-electrode array in either the median, radial, or ulnar nerve of each patient will be performed.

Milestone #1: Implantation of first patient. (Months 6)

Subtask 2.3: Micro-electrode array explantation (Months 9 – 36)

- Explantation of the micro-electrode array will be performed at the completion of the study (30 – 90 days post-implantation).

  0% complete.
  - *First subject has been identified, qualified, and consented for participation in the study. The micro-electrode array implantation and explantation can proceed if no-cost extension is approved.*

Major Task 3: Recording of isolated action potentials or multi-action potential activity from residual peripheral nerve while patient intends movements of amputated hand/arm

Subtask 3.1: Mapping of neural activity (Months 4 – 36)

- Patients will be asked to intend a number of individual finger and multiple finger flexion, extension, adduction, and abduction movements of their amputated hand by mimicking computer controlled movements of the virtual prosthetic hand. Similarly, they will be asked to make pronation-supination forearm movements; and flexion, extension, adduction, and abduction movements of their wrist.
- The spatio-temporal patterns of action potential firing evoked in the efferent fibers of the nerve will be recorded with the micro-electrode array during these intended movements. We will map the different intended movements onto the neural activity recorded on the electrodes of the micro-electrode array.

Milestone #2: chronic electrophysiological recording from first patient (Month 6)

25% complete.
- *The infrastructure for performing the electrophysiological recordings and simulation nerve mappings is in place and validated.*

Subtask 3.2: Offline analysis and decoding of movements (Months 6 – 36)

- Analyze the data recorded during sub-task 3.1 to determine if the neural activity can accurately predict the movements being intended.

50% complete.
- *The workstation computer and data server have been setup in the Goldwater Computing Center, and the offline analysis code have been implemented.*

Subtask 3.3: Online (real-time) decoding of movements (Months 6 – 36)

- Using data collected during subtask 3.1 we will train an online decode algorithm and then provide the patient real-time control over the virtual prosthetic hand.

Milestone #3: real-time control of multiple degree of freedom virtual prosthetic had in first patient (Month 9)

60% complete.

- *Computers for real-time computer analysis and control of the virtual prosthetic hand have been implemented in the patient cart. Real-time data acquisition, analysis, and control of the virtual prosthetic hand have been validated.*
- *The first subject has been trained on using the Vicon motion tracking system and the virtual reality environment.*

Major Task 4: Evaluation of somatosensory perceptions evoked by electrical micro-stimulation of the implanted nerve via the micro-electrode array

Subtask 4.1: Topographical mapping and subjective description of evoked perceptions (Months 6 – 36)

- We will perform electrical micro-stimulation at various currents on each electrode in the micro-electrode array in order to determine the minimum current needed to consistently evoke a sensory perception.

Subtask 4.2: Spatial two-point discrimination (Months 6 – 36)

- Using super-threshold micro-stimulation levels obtained in subtask 4.1, we will determine if micro-stimulation on pairs of electrodes with differing inter-electrode spacing evoke a single perception or two spatially distinct perceptions.

Subtask 4.3: Modulation of evoked perceptions (Months 6 – 36)

- We will determine if changes in micro-stimulation parameters result in modulation of the evoked sensory perceptions. We will provide modulation of micro-stimulation frequency using input from tactile sensors such as would be used in a prosthetic hand, i.e. micro-stimulation frequency would be modulated by the amount of pressure on a fingertip tactile sensor.

Milestone #4: Completion of studies and longitudinal analysis in all 6 patients. Preparation of manuscript for publication in scientific literature (Month 36)

30% complete.

- *The infrastructure for performing micro-stimulation to perform electrophysiological recordings and nerve mappings is in place and validated.*
- *We have incorporated biologically inspired micro-stimulation paradigms into the nerve mapping infrastructure based on evidence that they can evoke more naturalistic sensations.*

What was accomplished under these goals?

Our most significant progress has been on patient recruitment, training, and collecting baseline data. We have conducted outreach and information activities to orthopedic surgical centers. Through these activities we have identified and contacted 67 potential candidates, and then qualified and consented the first subject for the study.

Additionally, we have been making progress on activities and objectives related to 1) conducting the experiments on controlling the virtual prosthetic arm and providing sensory feedback to the subject, 2) improving the decoding algorithms for controlling the virtual reality prosthetic hand and the micro-stimulation paradigms for providing sensory feedback to the subject, and 3) improving the micro-electrode neural interface.

The cart of equipment of electrophysiological recording and micro-stimulation has been inspected and approved by the Biomedical Engineering department at the Mayo Clinic for recordings. We have of identified and tested specific rooms at the Mayo Clinic and at ASU for housing this equipment and performing the experiments with the patients. We have improved the virtual reality environment for patient training and real-time control of the virtual prosthetic hand using machine learning techniques.

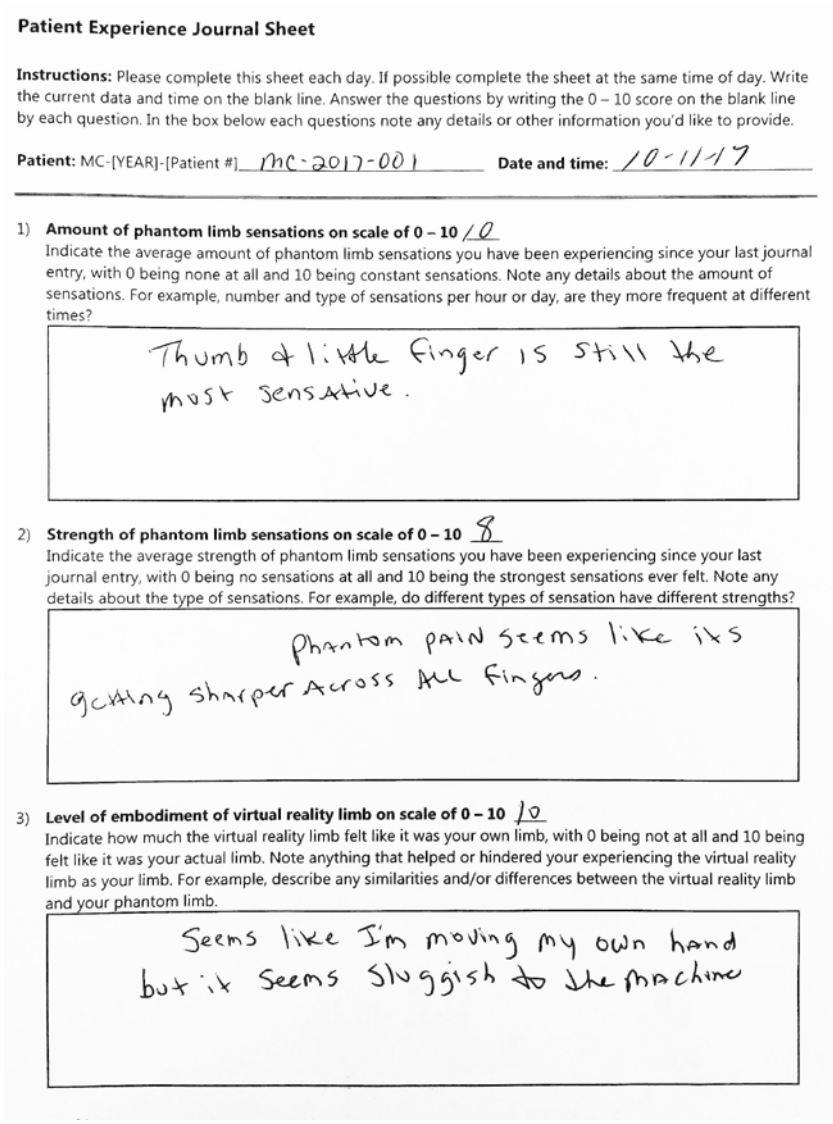

Patient Experience Journal Sheet

Instructions: Please complete this sheet each day. If possible complete the sheet at the same time of day. Write the current data and time on the blank line. Answer the questions by writing the 0 – 10 score on the blank line by each question. In the box below each questions note any details or other information you'd like to provide.

Patient: MC-[YEAR]-[Patient #] mc-2017-001 **Date and time:** 10-11-17

1) **Amount of phantom limb sensations on scale of 0 – 10** 10
Indicate the average amount of phantom limb sensations you have been experiencing since your last journal entry, with 0 being none at all and 10 being constant sensations. Note any details about the amount of sensations. For example, number and type of sensations per hour or day, are they more frequent at different times?

Thumb & little finger is still the most sensative.

2) **Strength of phantom limb sensations on scale of 0 – 10** 8
Indicate the average strength of phantom limb sensations you have been experiencing since your last journal entry, with 0 being no sensations at all and 10 being the strongest sensations ever felt. Note any details about the type of sensations. For example, do different types of sensation have different strengths?

Phantom pain seems like its getting sharper across all fingers.

3) **Level of embodiment of virtual reality limb on scale of 0 – 10** 10
Indicate how much the virtual reality limb felt like it was your own limb, with 0 being not at all and 10 being felt like it was your actual limb. Note anything that helped or hindered your experiencing the virtual reality limb as your limb. For example, describe any similarities and/or differences between the virtual reality limb and your phantom limb.

Seems like I'm moving my own hand but it seems sluggish to the machine

Figure 1 – Example page from the patient's journal. The patient documented his experience with the virtual reality prosthetic arm over 30 days.

We have identified and begun working with the first subject on the study. The has completed 30-days of working with and keeping a journal on his experiences with the immersive virtual prosthetic environment (Figure 1). Analysis of the movement data collected over the 30 days and the patient's journal reports will allows us to determine if practice with the virtual prosthetic hand immersive virtual reality environmental enabled the patient to "re-activate" their phantom limb. We have collected baseline movement data using the high-spatial resolution Vicon motion tracking system and performed the baseline nerve conduction study at Mayo Clinic (Figure 2). This baseline data will be compared with the data collect at the conclusion of the study to look for any chronic changes in movement control or nerve conduction.

Figure 2 – Training the first subject on using the Vicon motion tracking system. Two graduate students (Kevin O'Neil – left, and Cody Barton – right) are shown working with the first subject (center) of the study. The Vison motion tracking system was setup to work with the subject, and track the detail movements of his intact hand and the movement of his residual limb. This will allow the virtual prosthetic arm to be mapped onto, and move with his residual arm in the virtual reality environment of the Oculus Rift googles.

We have improved on past decoding efforts using machine learning algorithms based on multivariate time and frequency domain features. Patients and rehabilitation specialists have informed us that very high performing decoding algorithms are critical as even a few percent error translates into an unacceptable failure rate in object manipulation, e.g. dropping a utensil 5% of the time. The machine learning algorithms are being implemented on the patient cart for use in the real-time control of the virtual prosthetic hand experiments (Figure 3).

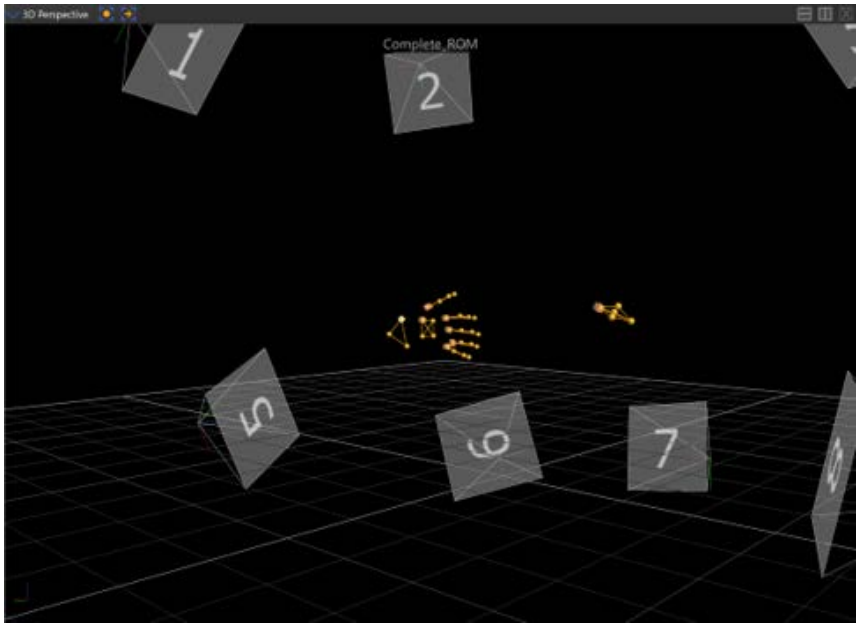

Figure 3 – Finger, hand, and limb position data collected from the first subject. The positions of the eight cameras of the Vicon motion tracking system are shown as gray, and the markers placed on the patient's hand and residual limb are show as yellow spheres. With this system we can with high spatial resolution both track the position of the fingers of the intact hand, and control the position of the fingers on the virtual prosthetic hand. Using the real-time data of the position of the residual limb we can have the virtual prosthetic hand move with the residual limb, aiding in the subject's sense of embodiment of the prosthesis.

Data from an earlier human study reveal challenges with using rigid silicon arrays in an active human patient population. The rigid silicon arrays were capable of making good electrophysiological recordings and performing micro-stimulation, however, they are susceptible to crush damage (Davis et al. Journal of Neural Engineering 2016). The use of compliant micro-electrode arrays will likely address this issue and provide path forward to long-term patient peripheral nerve interfaces. We have designed a compliant poly-LIFE micro-electrode array using Kevlar-fiber and cracked-gold materials that are similar to electrode arrays used successfully in previous human and animal studies that is resistant to crush damage. We have been seeking funding from other sources to develop the compliant poly-LIFE electrode arrays.

What opportunities for training and professional development has the project provided?

All of the students involved in the project have had extensive training and hands on experience on implementing the hardware (systems integration) and the software for offline analysis and real-time decoding and stimulation. They have had experience performing intraoperative electrophysiological neural recordings in human patients. They have been participating in all of the meetings with Mayo Clinic physicians, surgeons, and hospital staff.

How were the results disseminated to communities of interest?

The development of the improved virtual reality environment for patient training and improved decoding algorithms have been disseminated through presentations at scientific meetings, invited seminars, radio and television news programs, and peer-reviewed scientific publications.

What do you plan to do during the next reporting period to accomplish the goals?

Implant first and second subjects with currently approved electrode arrays, and conduct nerve mapping stimulation and electrophysiological recordings studies, i.e. Major Tasks 3 and 4. We will be recording electrophysiological signals from residual peripheral nerve while patient intends movements of amputated hand, and decoding these signals to control the virtual prosthetic hand. We will be stimulating the residual peripheral nerve to evaluate the subjective quality of the evoke somatosensory perceptions.

As the compliant ploy-LIFE arrays are develop, we will be seeking regulatory approval to use them with later human subject.

All of the infrastructure for performing the proposed work is in place and the first subject has been consented for performing the study, so if the no-cost extension is approved, the planned work can proceed immediately.

4. **IMPACT:**

What was the impact on the development of the principal discipline(s) of the project?

The development of the immersive virtual reality environment will enable new techniques and measurements of patient rehabilitation. We will be able to have patient practice with their virtual reality prosthetic hand prior electrode implantation. This will likely increase and improve the quality of the neural signals present in the residual nerve and thus improve the control over the prosthetic hand once the electrode array is implanted.

By using machine learning algorithms that utilize both time and frequency domain features we have improved the performance prosthetic control. To date control of advanced prosthetic hands have utilized linear decoding algorithms that do not incorporate the knowledge the most neural signals encode information in a nonlinear manner. These improved algorithms will likely increase patient acceptance of advance prosthetic hands, as even a few percent improvement in control translates into fewer unwanted movements, e.g. dropping a help object.

Providing sensory feedback of contact with grasped objects and/or the proprioceptive sense of finger position using micro-stimulation is important for patients' acceptance and use of the hand. Utilizing bio-inspired stimulation paradigms, i.e. stochastic stimulation that models the action potential firing rates of somatosensory transducing neurons in the skin versus non-stochastic machine-like stimulation, will likely result in more naturalistic perceptions. Generation of more naturalistic perceptions will also likely improve patients' sense of embodiment a prosthetic hand.

What was the impact on other disciplines?

The validation of algorithms for prosthetic control and stimulation paradigms for sensory feedback will aid progress in the fields of machine learning and bio-inspired design.

What was the impact on technology transfer?

Nothing to Report

What was the impact on society beyond science and technology?

This research has prompted several radio and television interviews on the use of neural prosthetic devices. These interviews provide the public with information about the benefits of this technology and the ethical issues that surround its use. Dr. Greger gaves interviews 01-Mar-2017 and 11-Apr-2017) on KJZZ (Phoenix Nation Public Radio station) on the topics of neural interfaces for rehabilitation and sensory restoration.

5. **CHANGES/PROBLEMS:**

Changes in approach and reasons for change

Given the high failure rate observed, we are planning in the long-term to switch to a more compliant electrode array technology that has a better chance of serving as platform for the long-term control of a prosthetic hand.

Actual or anticipated problems or delays and actions or plans to resolve them

Actual delays:
Ordering the currently approved electrode arrays has been intentionally delayed since a first subject for the study had not be identified. A first subject has been identified and consented for participation in the study, so ordering of the array can proceed.

Anticipated delays:
Patient recruitment is an unpredictable process. Identifying and recruiting the appropriate initial patient may result in delays. We have contact 67 potential candidates, and qualified one for participation in the study. We will continue to interact with this pool of candidates and seek to expand it through outreach activities.

Changes that had a significant impact on expenditures

No to report.

Significant changes in use or care of human subjects, vertebrate animals, biohazards, and/or select agents

None to report.

Significant changes in use or care of human subjects

None to report.

Significant changes in use or care of vertebrate animals.

Not applicable.

Significant changes in use of biohazards and/or select agents

Not applicable.

6. **PRODUCTS:** *List any products resulting from the project during the reporting period. If there is nothing to report under a particular item, state "Nothing to Report."*

Publications, conference papers, and presentations

Padamanaban S, Baker J, Greger B, Feature Selection Methods for Robust Decoding of Finger Movements in a Non-human Primate. Frontiers in Neuroscience – Neuroprosthetics, Research Topic on Artificial Intelligence and Brain Computer Interfaces 2018

Inventions, patent applications, and/or licenses

None to report.

Other Products

None to report.

7. **PARTICIPANTS & OTHER COLLABORATING ORGANIZATIONS**

What individuals have worked on the project?

Name:	*Bradley Greger*
Project Role:	*PI*
ORCID ID):	*0000-0002-6702-7596*
Nearest person month worked:	*2*
Contribution to Project:	*Dr. Greger has been overseeing as aspects of the project*
Funding Support:	*CDMRP, MTEC, NIH SBIR*
Name:	*Kevin O'Neil III*
Project Role:	*Graduate Student*
Researcher Identifier	
Nearest person month worked:	*7*
Contribution to Project:	*Kevin O'Neil III has been developing the VR prosthetic hand and immersive environment, and programing the patient cart*

Funding Support:	*CDMRP ASU, Dean's Fellowship*
Name:	*Subash Padmanaban*
Project Role:	*Graduate Student*
Researcher Identifier	
Nearest person month worked:	*2*
Contribution to Project:	*Subash Padmanaban has been developing machine learning algorithms*
Funding Support:	*CDMRP*
Name:	*Cody Barton*
Project Role:	*Graduate Student*
Researcher Identifier	
Nearest person month worked:	*1*
Contribution to Project:	*Cody Barton has been investigating the use of high-frequency power as an adjunct to action potential recordings for controlling prosthetic hands*
Funding Support:	*CDMRP, NIH SBIR*
Name:	*Denise Oswalt*
Project Role:	*Graduate Student*
Researcher Identifier	
Nearest person month worked:	*1*
Contribution to Project:	*Denise Oswalt had been developing and testing nonlinear support vector machines for decoding neural signals*
Funding Support:	*CDMRP, MTEC*

Has there been a change in the active other support of the PD/PI(s) or senior/key personnel since the last reporting period?

Nothing to Report.

What other organizations were involved as partners?

Mayo Clinic Arizona

8. **SPECIAL REPORTING REQUIREMENTS**

Not applicable.

9. **APPENDICES:**

- Padmanaban S, Baker J, Greger B, Feature Selection Methods for Robust Decoding of Finger Movements in a Non-human Primate, Frontiers in Neuroscience – Neuroprosthetics, Research Topic on Artificial Intelligence and Brain Computer Interfaces 2018.
  Paper provides information on implementation of machine learning algorithms for decoding finger movements.

- Davis T, Wark HAC, Hutchinson DT, Warren DJ, O'Neill III K, Scheinblum T, Clark GA, Normann RA, Greger B, Restoring motor control and sensory feedback in people with upper extremity amputations using arrays of 96 microelectrodes implanted in the median and ulnar nerves. Journal of Neural Engineering 13:3 2016.
  Paper provides information on earlier study and support for proposed changes to current work.

frontiers in Neuroscience

ORIGINAL RESEARCH
published: xx January 2018
doi: 10.3389/fnins.2018.00022

Feature Selection Methods for Robust Decoding of Finger Movements in a Non-human Primate

Subash Padmanaban[1]*, *Justin Baker*[2] and *Bradley Greger*[1]

[1] School of Biological and Health Systems Engineering, Arizona State University, Tempe, AZ, United States, [2] Viscus Biologics, Cleveland, OH, United States

Objective: The performance of machine learning algorithms used for neural decoding of dexterous tasks may be impeded due to problems arising when dealing with high-dimensional data. The objective of feature selection algorithms is to choose a near-optimal subset of features from the original feature space to improve the performance of the decoding algorithm. The aim of our study was to compare the effects of four feature selection techniques, Wilcoxon signed-rank test, Relative Importance, Principal Component Analysis (PCA), and Mutual Information Maximization on SVM classification performance for a dexterous decoding task.

Approach: A nonhuman primate (NHP) was trained to perform small coordinated movements—similar to typing. An array of microelectrodes was implanted in the hand area of the motor cortex of the NHP and used to record action potentials (AP) during finger movements. A Support Vector Machine (SVM) was used to classify which finger movement the NHP was making based upon AP firing rates. We used the SVM classification to examine the functional parameters of (i) robustness to simulated failure and (ii) longevity of classification. We also compared the effect of using isolated-neuron and multi-unit firing rates as the feature vector supplied to the SVM.

Main results: The average decoding accuracy for multi-unit features and single-unit features using Mutual Information Maximization (MIM) across 47 sessions was 96.74 ± 3.5% and 97.65 ± 3.36% respectively. The reduction in decoding accuracy between using 100% of the features and 10% of features based on MIM was 45.56% (from 93.7 to 51.09%) and 4.75% (from 95.32 to 90.79%) for multi-unit and single-unit features respectively. MIM had best performance compared to other feature selection methods.

Significance: These results suggest improved decoding performance can be achieved by using optimally selected features. The results based on clinically relevant performance metrics also suggest that the decoding algorithm can be made robust by using optimal features and feature selection algorithms. We believe that even a few percent increase in performance is important and improves the decoding accuracy of the machine learning algorithm potentially increasing the ease of use of a brain machine interface.

Keywords: feature selection, neural decoding, principal component analysis, non-human primate, support vector machine

OPEN ACCESS

Edited by:
Jennifer L. Collinger, University of Pittsburgh, United States

Reviewed by:
Dennis J. McFarland, Wadsworth Center, United States
Robert D. Flint, Northwestern University, United States

***Correspondence:**
Subash Padmanaban
spadman9@asu.edu

Specialty section:
This article was submitted to Neuroprosthetics, a section of the journal Frontiers in Neuroscience

Received: *23 February 2017*
Accepted: *11 January 2018*
Published: *xx January 2018*

Citation:
Padmanaban S, Baker J and Greger B (2018) Feature Selection Methods for Robust Decoding of Finger Movements in a Non-human Primate. Front. Neurosci. 12:22. doi: 10.3389/fnins.2018.00022

INTRODUCTION

Microelectrode array brain machine interfaces (BMI) have shown the potential to alleviate various neurological disorders. BMIs utilizing advances in robotics and machine learning can restore limited lower and upper extremity motor function. Several research studies have investigated the viability of a cortical brain machine interface in humans and NHPs (Musallam et al., 2004; Kim et al., 2008; Gilja et al., 2012, 2015; Collinger et al., 2013; Hwang and Andersen, 2013; Aflalo et al., 2015). BMI for controlling a robotic limb or moving a cursor have been successfully demonstrated in humans and non-human primates (NHP). These systems provided real time control of a neuroprosthetic system by decoding neural signals moment by moment with an objective to provide certain functionality to replace the native arm. These systems are based on decoding the endpoint goal of reach and map the neural signals to spatially distributed targets. Wang et al. (2009) decoded individual finger movements using neural data recorded using a customized micro-ECoG grid. The quality of neural data was analyzed by using frequency domain based characteristics like coherence between different electrodes, modulation of neural signals and accuracy of finger movement classification. Shenoy et al. (2007) developed a finger movement classification algorithm based on neural data recording using Electrocorticographic BCI. The classification error achieved using this real-time BCI was 23%. Kubánek et al. (2009) also demonstrated the ability to decode the time course of individual finger flexions based on ECoG signals recorded from the motor cortical region in human subjects. Graimann et al. developed a wavelet packet analysis and genetic algorithm for detecting ERPs in a single channel ECoG brain computer interface. Bashashati et al. (2007) and Garrett et al. (2003) provide a comprehensive review of feature selection methods in EEG-based brain computer interfaces.

BMIs can be broadly classified based on the type of bio-signal used to control the prosthesis. Electroencephalogram (EEG), Local field potential (LFP), and Action potential (AP) constitute the majority of source signals used in BMI. APs are discrete spiking events of an individual neuron. In statistics terms, APs or neural "spiking" can be thought of as a non-stationary point process in which neural information is largely encoded by changes in the AP firing rate coding (frequency of APs/spiking) (Truccolo et al., 2005). In this paper, we utilize neural recordings of APs from individual neurons to classify various movements of the fingers. One of the important characteristics of the human upper extremity functioning is the ability to perform coordinated and dexterous finger movements. Typing, eating with a spoon, writing with a pen and opening a lock with a key are some of the examples in our daily life that require such dexterous manipulations using individual or combined finger movements. Incorporating dexterity as a feature in a neuroprosthesis would help amputees and paralyzed persons to carry out a wider range of tasks. To achieve such dexterous control requires a neural decoding algorithm that can map high-dimensional neural signals onto a high-dimensional hand prosthesis. Optimizing algorithms for decoding neural signals will be critical for providing useful control of upper extremity neuroprosthesis. Feature selection is an important step in designing a machine learning system. Choosing a *O*-dimensional subset from a *P*-dimensional feature space consisting of "*P*" predictors using an objective metric is the aim of feature selection. Feature selection also reduces the dimensionality of feature space, inundating it with more "informative" features thus, removing lesser contributing ones that might occlude the feature space.

Curse of Dimensionality

Certain machine learning algorithms fail to scale well in high dimensional feature space. These algorithms suffer from the "curse of dimensionality," which refers to the problems that arise when analyzing and organizing high-dimensional data. Consider a univariate, independent variable "X" which follows a Gaussian distribution with mean "μ" and variance "σ" ($X \sim N(\mu, \sigma)$). According to the properties of Gaussian distribution, ∼68% of the data is enclosed in the region surrounded by the mean ± 1 standard deviation (**Figure 1A**). Consider two independent variables X_1 and X_2 which follow Gaussian distributions with means "μ_1" and "μ_2," and variances "σ_1" and "σ_2" respectively ($X_1 \sim N(\mu_1, \sigma_1)$ and $X_2 \sim N(\mu_2,\sigma_2)$). For a bivariate, Gaussian distribution only ∼40% of the data is enclosed within the same region (**Figure 1B**). For a 50-dimensional multivariate normal distribution, only ∼1/250,000,000th of the data lie within the mean ± 1 standard deviation region. As the number of dimensions (variables) increase, the amount of data bounded by the mean ± 1 standard deviation region decreases exponentially (**Figure 2**). In neural decoding, data from each electrode is treated as an individual feature. A microelectrode array usually consists of 96 electrodes thus, making the feature space 96-dimensional. In case of a 96-dimensional feature space, only an infinitesimally small proportion of data points are enclosed in the mean ± 1 standard deviation region. Results of **Figure 1** were generated using a novel approach to constructing the Multi-dimensional standard deviation ellipsoid based on spectral decomposition of the sample covariance (Wang et al., 2015).

In high-dimensional space, almost every point is closer to the edge of a hypercube that encloses the points than to another sample point. For a sample of size "n," the expected average distance between the sample points and the edge of the hypercube "D" in a "d"-dimensional feature space can be estimated using the following equation:

$$D(d,n) = \frac{1}{2}.\left(\frac{1}{n}\right)^{\frac{1}{d}}$$

For a two-dimensional space with 10,000 points, the average expected distance between the sample points is 0.005 and for a 100-dimensional space with the same number of points, the expected distance is 0.45. It should be noted that the maximum distance from any point to the edge is 0.5 for normalized values of dimensions (Kantardzic, 2011). The expected distance asymptotes to 0.5 when the number of dimensions approaches infinity.

It can be seen that the percentage of data points enclosed by the mean ± standard deviation region decreases as the number

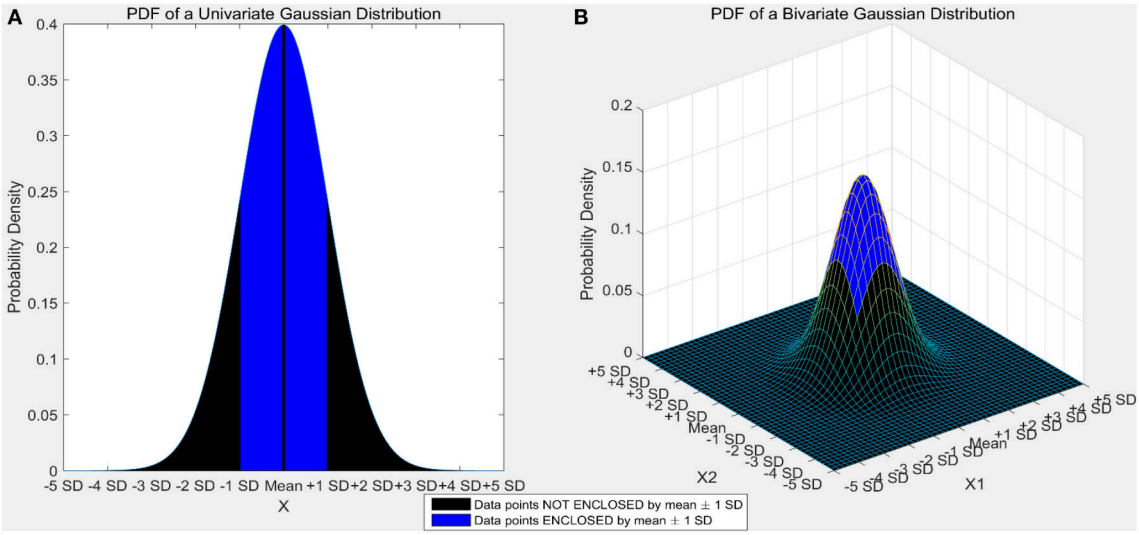

FIGURE 1 | (A) Univariate gaussian distribution. The area shaded in red shows the data points bounded by mean ± 1 standard deviation. 68.27% of the data is enclosed in this region. **(B)** Bivariate Gaussian distribution. The area shaded in blue shows the data points bounded by mean ± 1 standard deviation. Only 39.35% of the data is enclosed in this region. As the number of dimensions increase from a univariate to a bivariate distribution, the amount of data bounded by mean ± 1 standard deviation reduces by ∼42%.

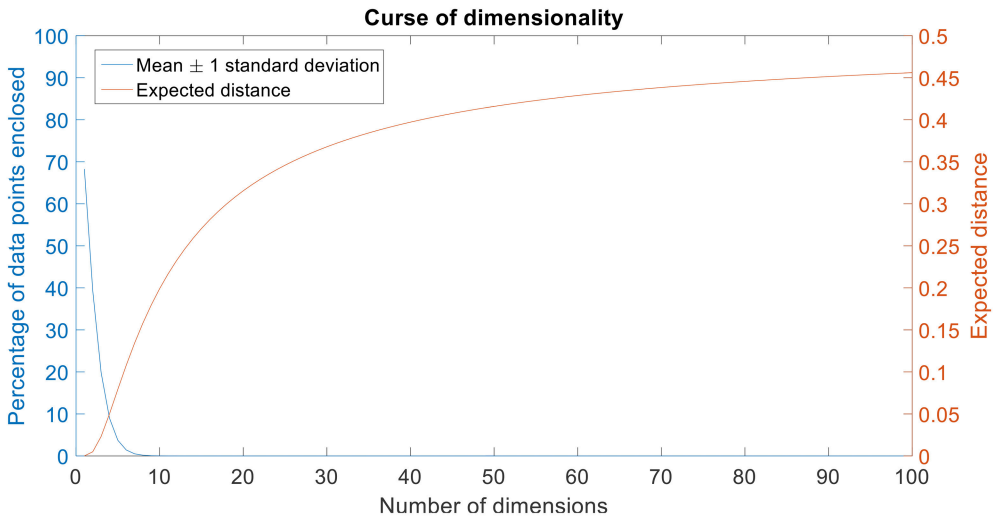

FIGURE 2 | Curse of dimensionality. The plot in blue shows the percentage of data points enclosed by the mean ± 1 standard deviation for 100 dimensions. The amount of data enclosed by the mean ± 1 standard deviation region asymptotes to zero from an octa-variate (8-dimensional Gaussian distribution contains only 0.18% of the data in mean ± 1 standard deviation region) distribution. The plot in red shows the expected distance for 100 dimensions. Expected distance is defined as the average distance between the sample points and the edge of a hypercube. The expected distance asymptotes to its maximum value of 0.5 as the number of dimensions increases.

of dimensions increase (**Figure 2**). Also, the expected distance increases quadratically (and asymptotes toward its maximum value, 0.5) as the number of dimensions increase (**Figure 2**).

The above two examples illustrate the sparsity of finite data in high-dimensional space. In high-dimensional space, most data points act as outliers. This sparsity in data distribution deters the efficacy of certain machine learning algorithms in high-dimensions. Feature selection is one of the methods to cope with "curse of dimensionality."

Using machine learning algorithms for multivariate, high-dimensional data is often computationally expensive. Due to the complexity of feature space and rigorous numerical computations involved in defining the hyperplane in this high-dimensional feature space, the performance of the machine learning algorithm is deterred. Feature selection is the process of selecting an *O*-dimensional subset feature space from a *P*–dimensional original feature space where "*p*" is the number of predictors.

Feature selection is usually applied to reduce information redundancy and trim the input space to better predict the responses. Some of the advantages of feature selection are:

- Facilitate data visualization and data understanding
- Reduce data measurement and storage requirements
- Reduce training and utilization times
- Simplify the learning model and aid in better understanding and interpretation by researchers
- Enhance generalization by reducing overfitting
- Defy the curse of dimensionality to improve predictor performance (Guyon and Elisseeff, 2003).

Identifying the best subset of features is a time consuming and resource intensive problem to solve. The only method to do this is through exhaustive grid search, i.e., exhaustively searching through every permutation of predictors available. Mathematically, there exists 2^p permutations of features that can be selected from "p" features. In case of our neural data, this results in iterating through 2^{96} (96 features for multi-unit firing rate and >96 features for single-unit firing rate based feature vector) permutations of features to identify the "best" subset.

When dealing with multivariate, time-series signals like neural signals, it is imperative to judge where the learning algorithm must focus its attention. *Filter* or *Criterion* based feature selection and *Wrapper* based feature selection are two broad categories of feature selection that are commonly applied in machine learning (Kohavi and John, 1997). Application of statistical, empirical or other "criteria" based methods such as mean, variance,

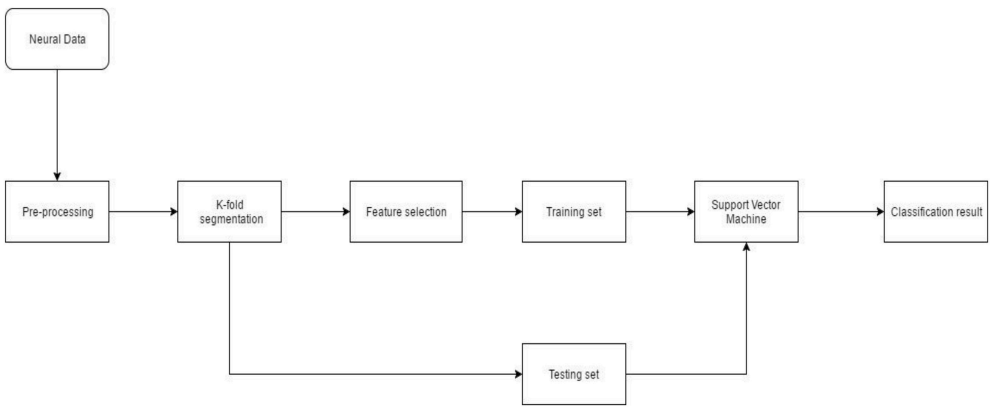

FIGURE 3 | Neural decoding system architecture. After pre-processing the neural data, feature selection was performed. During K-fold segmentation, the entire data set was divided into 10-folds. 9-folds were used for training and the 10th-fold was used for validation. This process was repeated 10 times until each fold served as a validation fold. The 9-fold training data was further divided into 3-folds for parameter estimation of the SVM. Validation error and parameters of the SVM were estimated using a nested cross-validation loop.

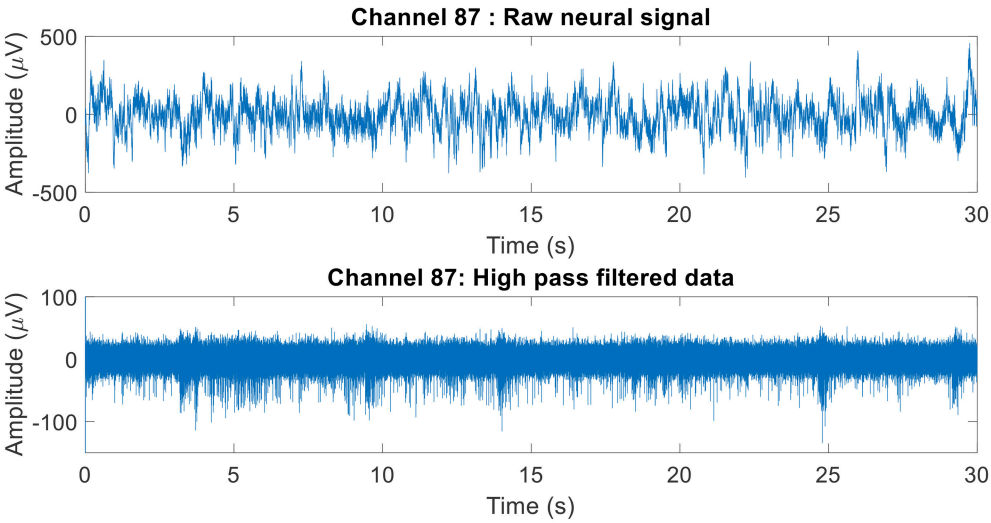

FIGURE 4 | Raw neural recording on channel 87. The 30 s recording consisted of multiple different trials. The raw neural recording on each was filtered using a high-pass Butterworth of cut-off frequency 250 Hz (channel 87 was chosen at random). The MATLAB function "*filtfilt*" was used to filter the neural signal to ensure zero-phase distortion.

student's *t*-test and correlation are some examples of criterion based feature selection. Applying criterion based feature selection requires some domain expertise in order to determine what qualifies as a useful criteria. Wrapper based feature selection iteratively uses various combinations of features as input to a machine learning algorithm and evaluates the importance of each feature based on some evaluation criteria from the prediction such as coefficient of determination (r^2). Ideally, it is advisable to use the same machine learning algorithm as a classifier and a wrapper for feature selection. Oftentimes, it is also valuable to use a simpler, computationally efficient machine learning algorithm as a substitute wrapper. For example, SVMs are an efficient but computationally intensive solution to solve the problem of face recognition by computing key points (that act as features) on the face. Using SVM as a wrapper in this case would demand access to a lot of resources (in terms of clusters) and still be time consuming. An alternative to using SVM in this case would be using a simpler algorithm such as Logistic

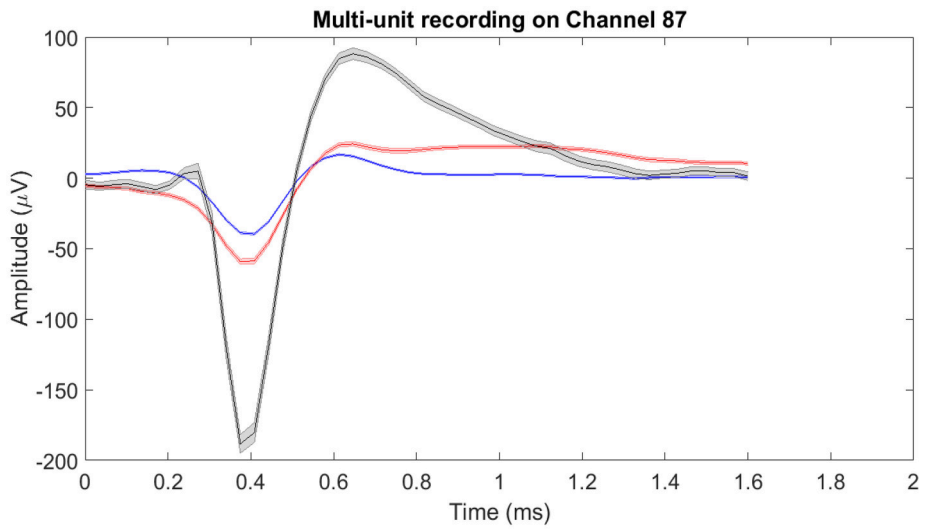

FIGURE 5 | Mean of isolated single-units neural activity on Channel 87. Channel 87 contained three individual single-units post-spike-sorting. Since there was more than one single-unit recorded on channel 87, the single-unit and multi-unit firing rates were different. For single-unit firing rate, each single-unit was treated as an individual source of information. Whereas for multi-unit firing rate, the single-units were treated as one and the firing rate was computed. The shaded region around the mean action potential corresponds to the standard error of the action potential waveforms.

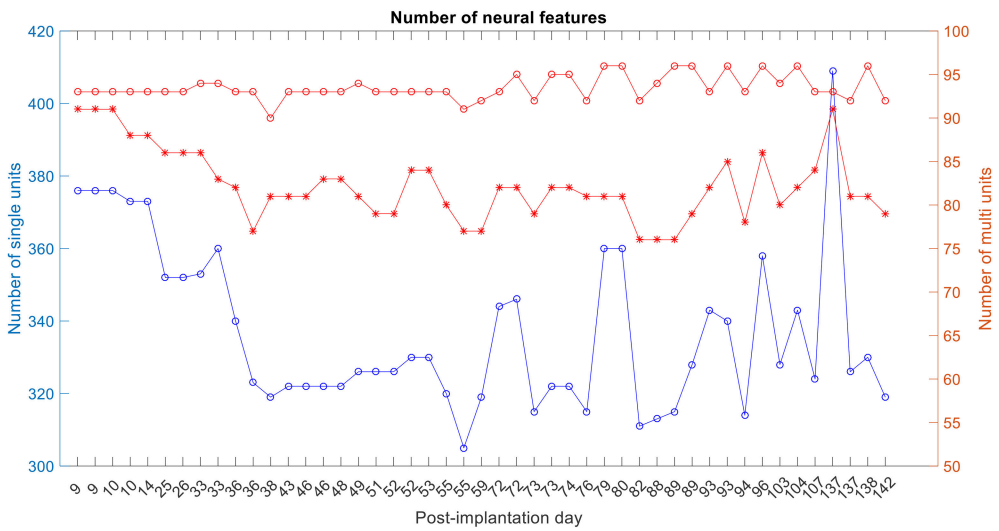

FIGURE 6 | Number of single-unit features, multi-unit features and number of active electrodes with any neural activity. The blue plot corresponds to the number of isolated single units, red-asterisk plot corresponds to the number of active electrodes with multi-unit activity and the red-circle plot corresponds to the number of active electrodes with any neural recording (single and/or multi-units).

regression. Care should be taken to ensure both the algorithms have similar assumptions about the data such as nonlinearity or heteroscedasticity of noise.

METHODS

Approval for the animal use protocol in this study was obtained from the University of Utah Institutional Animal Care and Use Committee (IACUC). All procedures conformed to National Institute of Health (NIH) standards for animal care. The recording setup, behavioral task, data collection and preliminary data processing approaches are explained elsewhere (Baker et al., 2009). A 96 channel microelectrode array (MEA, Blackrock Microsystems) was implanted in the hand area of primary motor cortex of a male macaca mulatta. The NHP was trained to perform cued combined flexions of the thumb, index and middle finger and individual flexions and extensions of the same digits using a manipulandum. Visual cues were provided using a computer screen placed in front of the monkey. In order to start a trial, the monkey had to relax all its fingers moving all of the finger switches in the manipulandum to the open state. After a randomized wait time of 1,000–3,000 ms, a visual cue indicating which finger(s) to flex/extend appeared on the computer screen. The monkey then had 2,000 ms to react to the visual cue and depress the associated switch. Once the correct switch was pressed, the monkey had to hold the switch for 500 ms. The trial was deemed successful if the monkey pressed the correct switch and adhered to the time constraints. The behavioral task was implemented using a real-time operations systems in a custom LabVIEW (National Instruments) program.

Neural Decoding System Architecture

Neural data recorded from the NHP was spike sorted. The timestamp of spike events was obtained from the offline sorter. Pre-processing also included binning/moving average windowing of the point process using a boxcar window. After applying the moving average technique, neural "firing rate" for each single or multi-unit was obtained. Neural firing rate was used as the feature vector (input) to the SVM. Neural activity corresponding to each successful finger movement trial was extracted and concatenated. The entire dataset was randomly divided into 10-folds. Each fold served as the testing set once while data from the remaining folds was used for training. Model parameters such as box constraint(C) and sigma (for the RBF kernel) were estimated using an exhaustive grid search algorithm with exponentially increasing values from 1e-5 to 1e5. Classification accuracy was calculated after predictions were made on the unseen test set. This process was repeated 20 times to reduce generalization error of the SVM (**Figure 3**).

Pre-processing

The MEA is a 10 × 10 grid of 1 mm tall electrodes that are capable of recording APs in addition to LFPs (House et al., 2006). The MEA data were sampled at 30 kHz. Neural data collected using the MEA were sorted offline using an expectation-maximization based competitive mixture of *t*-distributions decomposition algorithm (Shoham et al., 2003). Data were then imported to Matlab (Mathworks) for further analysis. The time stamps of APs recorded at 30 kHz were downsampled to 600 Hz. A boxcar moving average window of 300 ms width and 33.3 ms step size was used to obtain a moving average firing rate (Davis et al., 2016). Electrodes in the motor cortex can record from more than one neuron. The features extracted from neural signals recorded from such electrodes are called "multi-unit" firing rate. However, the neural activity recorded on such electrodes can be separated using techniques such as Principal Component Analysis (PCA), Expectation-Maximization algorithm or Independent Component Analysis (Lewicki, 1998). Features extracted from such individual, isolated neurons are called "single-unit" firing rate. The moving average firing rate was downsampled in order to reduce data size. A 4th order low pass Butterworth filter with a cut-off frequency of 10 Hz was used prior to downsampling the neural firing rate to

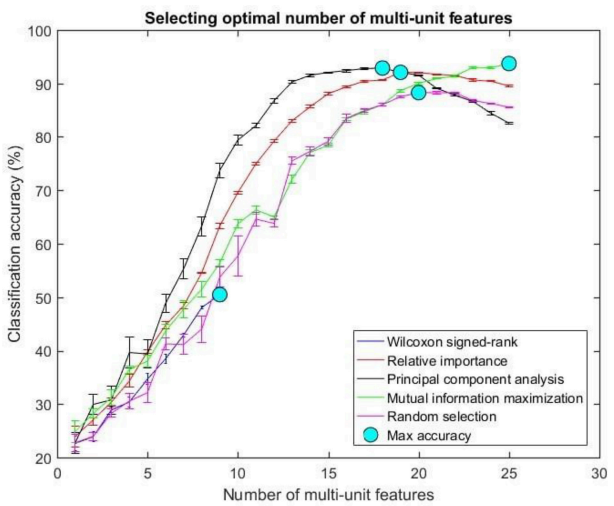

FIGURE 7 | Selecting optimal number of multi-units. The plot above shows the cross validated accuracy of feature selection algorithms for increasing number of multi-unit features. The solid circle (cyan) in each graph shows the maximum cross-validated accuracy for a feature selection algorithm. The number of single or multi-unit features corresponding to this accuracy was chosen as the optimal number of features. The points and error bars correspond to the mean and standard error of maximum cross-validated accuracy respectively.

TABLE 1 | Feature selection algorithms and their respective optimal number of features on post-implantation day 36.

	Wilcoxon signed-rank test	Relative importance	PCA	MIM	Random features
Multi-unit	9 (50.48%)	19 (92.07%)	18 (92.88%)	25 (93.71%)	20 (88.28%)
Single-unit	19 (89.84%)	21 (90.53%)	16 (93.19%)	25 (95.71%)	17 (85.27%)

20 Hz and the neural firing rate was obtained as a time varying vector. This process was repeated for all 96 electrodes to obtain multi-unit neural firing rate, i.e., the cumulative firing rate of all neurons recorded on a particular electrode. An average of 142.2 ± 36.3 neural units were recording from 96 electrodes during each session. Spike-sorting was performed on all neural data for each experimental recording session separately from other recording sessions.

Data from individual trials was aligned in time on switch closure times of successful trials. A movement period was defined as the duration corresponding to 450 ms prior and 1,000 ms after the switch closure. A baseline period (resting state) for a trial was defined as the duration corresponding to 2,500–1,000 ms prior to switch closure. Baseline and movement period data was obtained for all available degrees of freedom and all successful trials for each day experiments were conducted and represented a vector of time-series data.

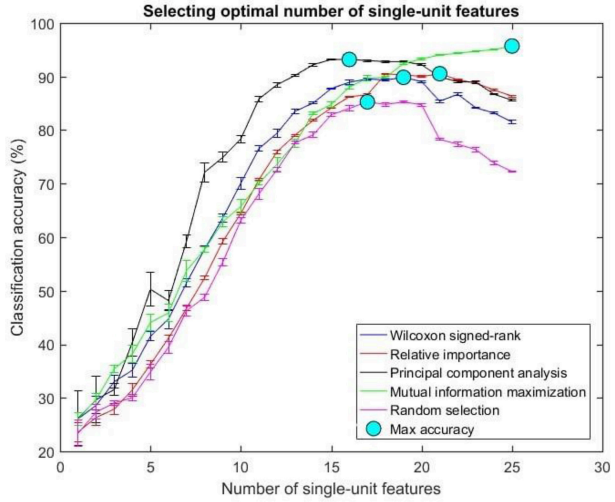

FIGURE 8 | Selecting optimal number of single-units. The plot above shows the cross validated accuracy of feature selection algorithms for increasing number of single-unit features. The solid circle (cyan) in each graph shows the maximum cross-validated accuracy for a feature selection algorithm. The number of single or multi-unit features corresponding to this accuracy was chosen as the optimal number of features. The points and error bars correspond to the mean and standard error of maximum cross-validated accuracy respectively.

Feature Selection

In this study, we have limited our comparisons to criteria based feature selection methods.

Wilcoxon Signed-Rank Test

Wilcoxon signed-rank test is a non-parametric alternative to the student's *t*-test. This non-parametric test can be used to identify if samples from two independent yet related distributions are significantly different (Randles, 1988). In the context of selecting single or multi-unit data as input to the SVM, the difference between baseline and movement related firing rate was computed. The null hypothesis was that the data came from a continuous, symmetric distribution with a median equal to zero (i.e., no electrode recorded increased firing rates in the movement period as compared to the baseline period). Electrodes for which the null hypothesis was rejected ($p < 0.001$) with a positive median difference from baseline were kept. These electrodes were then sorted in order of increasing median difference. For the purpose of feature selection, the median difference was computed as a scalar to select features (single unit/multi-unit).

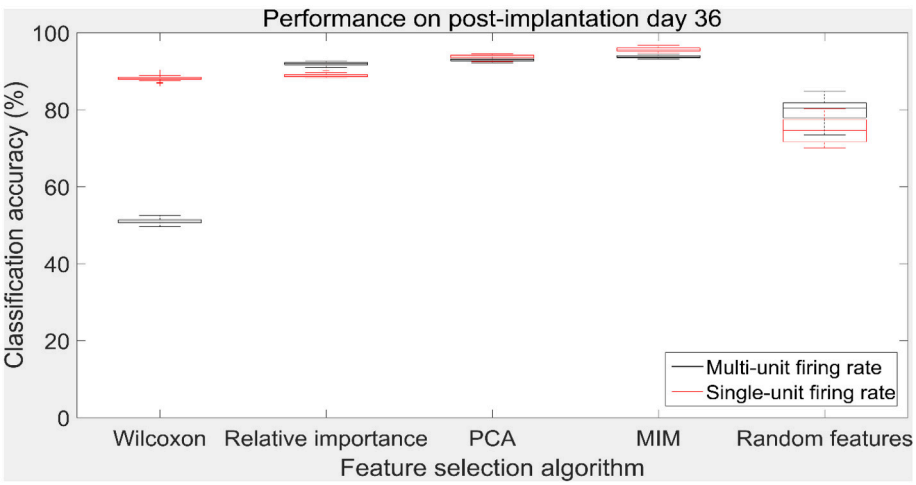

FIGURE 9 | Accuracy of neural decode on post-implantation day 36. Classification accuracy of feature selection algorithms on the test set using cross validated optimal number of features. The plots in black and red correspond to classification accuracy obtained using multi-unit firing rate and single-unit firing rate respectively. Level of chance was 10% (10 degrees of freedom). The central box represents the central 50% of the data with the top and bottom sides of the central box representing the 75% quantile and 25% quantile respectively. The central line in the central box represents the median of the central 50% of the data. The vertical lines extending above and below the central box represent the remaining data that are not regarded as outliers.

Relative Importance

Relative importance was a feature selection technique initially developed for selecting neurons in the primary motor cortex for decoding (Kim et al., 2012). First the movement only firing rate (difference of movement and baseline firing rate) was computed. The trial averaged firing rate for each neuron for all the successful trials was calculated. Then, the inter-movement variance was computed as the difference of trial averaged firing rate and the average firing of a neuron for a particular movement. The neural recordings were then ranked in descending order of inter movement variance. For the purpose of feature selection, the inter movement variance was computed as a scalar to rank features (single/multi-unit).

Principal Component Analysis

PCA can be used as a feature transformation technique, where a transform function is applied to the data to represent it in a higher dimensional transform space. For an "*n*" dimensional possibly correlated data, PCA represents the data in a (n−1) dimensional space in linearly uncorrelated principal component coordinates (Jolliffe, 2002; Lu et al., 2007). The transformation is carried out in such a way that the first principal component contains the maximum possible variance of the data. The succeeding principal components are ordered in descending order of variance. This transformation of data according to the variance at each time point can be used to eliminate noise, but does not necessarily extract discriminative features. Neural firing rates corresponding to each movement was provided as an input to PCA. The operation of PCA can be thought of as revealing the internal structure of the data based on its variance. For a multivariate dataset that can be represented in a high-dimensional space, PCA provides a better representation in low-dimensional space from an "informative" viewpoint. This is done by considering only the first few principal components and thus, PCA serves as a dimensionality reduction method. The features extracted using PCA were ranked based on the amount of variance explained by the individual principal components.

Mutual Information Maximization

Mutual information is the mutual dependence of two random variables. Unlike correlation, mutual information is not limited to real-valued random variables and estimates how similar the joint distribution P(X|Y) is to the products of the factored marginal distribution P(X) and P(Y) (Torkkola, 2003). Entropy of a random variable C can be defined as:

$$H(C) = -\sum_{c} P(c) \log(P(c))$$

The conditional entropy of two random variables C and Y can be defined as:

$$H(C|Y) = -(\sum_{c} P(c|y) \log\left(P(c|y)\right) dy$$

Then, the mutual information of random variables C (neural firing rate) and Y (movement type) can be defined as the I(C;Y) = H(C) – H(C|Y) and can be represented as:

$$I(C|Y) = \sum_{c} \sum_{y} P(c|y) \log \frac{P(c|y)}{P(c) * P(y)}$$

Mutual Information maximization (MIM) was implemented using the FEAST Toolbox available for MATLAB (Brown et al., 2012). For a class label Y, the mutual information score of feature C is defined as:

$$J(C) = I(C|Y)$$

This score J(C) is referred to as MIM and we rank the features in descending order of the mutual information score. Neural firing rates corresponding to movement period for each degree of freedom was used as the input to MIM algorithm.

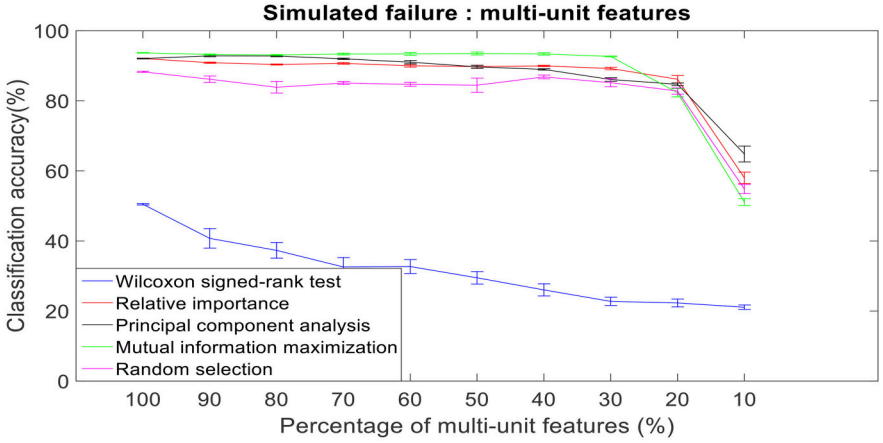

FIGURE 10 | Robustness to simulated failure of multi-unit features. The plot above shows the cross-validated classification accuracy at various failure levels. Error bars indicate standard error of the cross validation folds.

Support Vector Machine

Support vector machines (SVM) have shown promising results in upper extremity decoding tasks using various source signals such as MEG, EEG, ECoG, and EMG (Bitzer and van der Smagt, 2006; Demirer et al., 2009; Quandt et al., 2012; Wissel et al., 2013). SVM is a class of non-probabilistic, binary, linear classifier (Platt, 1999). SVMs represent the data in higher dimensional space and find the best separating hyperplane in this space. The objective of the SVM is to find a hyperplane that has the maximum distance from a point belonging to any class. Such a classifier is also called a maximum margin classifier whose generalization error is low. During training, each point in the training set is assigned a weight α. Those points with training weights $\alpha \neq 0$ are called the support vectors since, they help forming the hyperplane. In case of linearly non-separable cases, a soft margin classifier is implemented which allows for misclassified instances. Non-linear problems can be solved by using the "kernel trick" in the SVM. Kernel functions map data into a higher dimensional space where, the hyperplane is now formed. Gaussian (radial basis function) kernel was employed in our classification problem to account for non-linearity in the input-output relationship. Gaussian kernel K(x,x') for two samples x and x' defined as a feature vector in some predictor space is defined by:

$$K\left(x, x'\right) = exp\left(-\frac{||x - x'||^2}{2\sigma^2}\right)$$

where σ is a free parameter that defines the smoothness of the Gaussian kernel.

SVMs are inherently binary classifiers, i.e., they can distinguish between only two classes. Their functionality can be expanded to solve multiclass problems by decomposing it into multiple binary sub-problems (Hsu and Lin, 2002; Duan and Keerthi, 2005). We used a one-vs.-one multiclass implementation of the SVM to differentiate between the many available movements. For a problem of classifying "k" classes, we require $\frac{k(k-1)}{2}$ binary SVM classifiers for each pair of the "k" classes. The class of a test instance is predicted by taking the mode of predictions of all the one-vs.-one SVM pairs.

In addition to extracting neural activity corresponding to valid trials for all available degrees of freedom for a particular session, we included 30 random baseline periods as a "rest" phase (11th degree of freedom). During the training phase of supervised learning algorithms such as SVM, the algorithm must be provided with corresponding outputs (class labels). The class labels were created depending on the movement type. For example, thumb flexion was encoded as 1, index flexion as 2, middle finger flexion as 3 and so on.

Performance Metrics

The first step in assessing the performance of feature selection methods was to find the optimal number of features for each feature selection algorithm that best classified the different finger movements and the resting state. For this purpose, all available successful trials in a session were split into a 70% for training and the remaining 30% for testing. A 10-fold cross validation routine was performed to reduce variability in performance estimates during validation. For a given input data (multi-unit or single-unit firing rate), the features were ranked based on the results of the feature selection algorithms. The extracted features were ordered and selected in a descending order based on their ranking by each feature selection method with the best features being selected first. We iteratively incremented one feature (neural firing rate on a single electrode or from an isolated neuron) at a time and used it as an input to the classifier to identify the optimal number of features. In order to evaluate the performance of features selected at random, we also included random multi-unit and

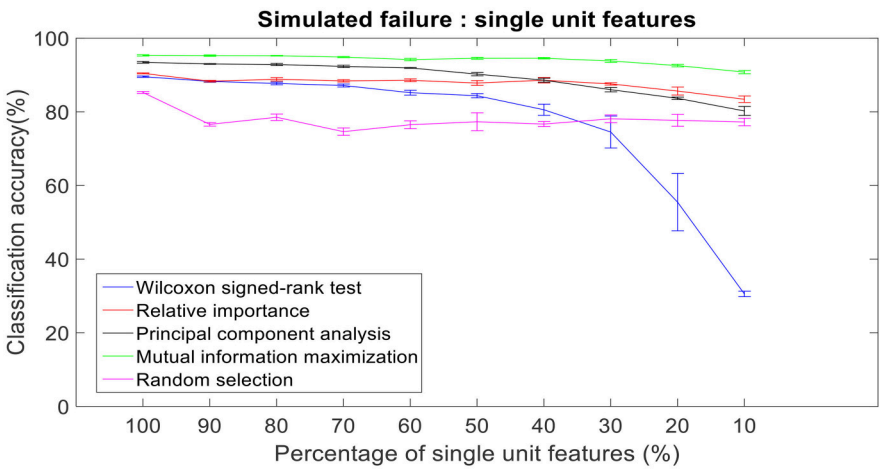

FIGURE 11 | Robustness to simulated failure of units. The plot above shows the cross-validated classification accuracy at various failure levels. Mutual information maximization based feature selection had a classification accuracy of 90.79% with just 10% of the neural units as feature vector. Error bars indicate the standard error of classification accuracy.

isolated unit firing rate feature to compare with the other methods.

Robustness to Simulated Failure

The performance of the brain machine interface (BMI) can be influenced by the quantity of neural information available for decode. Previous research has shown that there is a significant decrease in the signal to noise ratio of the neural signals and a steady decrease in impedance of the recording electrodes over time (Vetter et al., 2004; House et al., 2006). There can be a steady decrease in the number of electrodes that record APs, which can have a deleterious effect on BMI performance. AP recordings can also be affected due to glial scarring or electrode location changes (Frien and Eckhorn, 2000; Leopold and Logothetis, 2003; O'Leary and Hatsopoulos, 2006; Stark and Abeles, 2007; Berens et al., 2008; Jia et al., 2011). Feature selection algorithms should be robust enough to handle the sudden losses in neural information over time. In order to test the endurance of the feature selection algorithms, we randomly dropped 10's of percent of the available neural firing rate and tested its performance. The random removal procedure was repeated 20 times to reduce generalization bias.

Longevity of Neural Decodes

BMI are devices which will be used over an extended period of time. In order to be useful the neuroprosthetic device must be capable of accurate performance over this extended period of time. We present here the chronic decoding results of 47 sessions collected over 142 days. Spike-sorting was performed individually on each of the 47 sessions. For a given session the optimal number of features was computed. Decoding accuracy for a feature selection algorithm on a particular day was then calculated using the cross validated optimal features.

RESULTS

Quality of Neural Recordings

The raw neural data was high-pass filtered using a Butterworth filter with a cut-off frequency of 250 Hz (**Figure 4**). To demonstrate the quality of neural recordings used in this analysis, we extracted a 30 s neural recording on a randomly selected channel (channel 87). PCA followed by k-means clustering was performed to separate the isolated units and noise. In Channel 87, there were 3 isolated single-units (**Figure 5**). Single-unit firing rate was obtained by treating the isolated neural units as individual sources of information. Therefore, we obtained three single-unit firing rates for channel 87 by treating single-units 2, 3, and 4 as individual sources of information. Multi-unit firing rate was obtained by treating the individual single-units as one source of information. Therefore, we accrued the neural activity of the single-units and obtained one multi-unit firing rate for channel 87. To summarize, the number of multi-unit features is equal to the number of active electrodes (irrespective of the number of isolated units it was recording). Whereas, the number of single-unit features is equal to the number of isolated units. Spike sorting was performed individually on all data from each session.

The number of single and multi-unit features was calculated (**Figure 6**). For the 1st session on post-implantation day 9 there were 92 electrodes (red-circle plot; out of a possible 96) with any neural activity (single and/or multi-unit recordings), 89 electrodes (red-asterisks; out of 92) had multi-unit recordings, i.e., more than one isolated single unit, and 378 isolated-single units (on the 92 electrodes).

Selecting Optimal Number of Features

The optimal number of features for various feature selection algorithms on post-implantation 36 was differing (**Table 1**). The

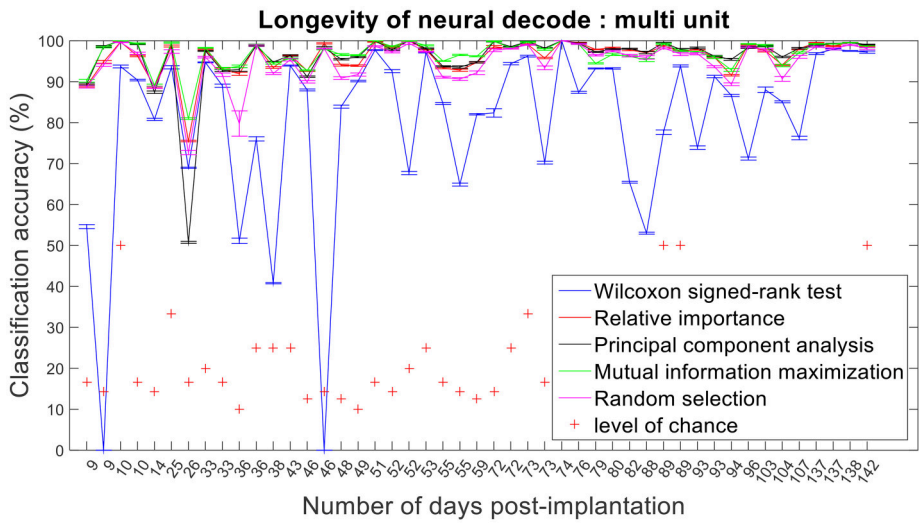

FIGURE 12 | Longevity of neural decodes using multi-unit firing rate. High levels of accuracy over an extended period of time is imperative for a fully functional neuroprosthesis. On certain days, two sessions of recordings were conducted. Repeated x-axis indices (Number of days post-implantation) in the above figure correspond to different sessions conducted on the same day.

classification accuracy for incremental values of number of features was plotted (**Figures 7**, **8**).

The values in **Table 1** correspond to the optimal number of features (values outside the parentheses) and maximum cross-validated accuracy (values within the parentheses). With an exception of Wilcoxon signed-rank test, the other feature selection algorithms did not show significant changes (two sample t-test, $p < 0.05$) from using multi-unit and single-unit firing rate both in terms of number of optimal features and classification accuracy (less than $\pm$ 3% difference in classification accuracy and $\pm$ 1 feature). In case of Wilcoxon signed-rank test, the number of optimal features increased from 9 features for multi-unit firing rate to 19 feature for single-unit firing rate. The classification accuracy improved from 51.12 $\pm$ 0.65% for multi-unit firing rate to 88.12 $\pm$ 0.61% for single-unit firing rate (**Figures 7**, **8**). The number of optimal features for multi-unit features using Wilcoxon signed-rank test stops at 9 features because this feature selection methods returned only 9 multi-unit features as having a significant difference between the movement and baseline period.

The performance of the various feature selection methods was analyzed on a randomly selected session (post-implantation day 36). On post-implantation day 36, MIM performed significantly better than the other algorithms and random selection (two sample t-test, $p < 0.05$, α – values calculated using Bonferroni correction to account for multiple comparisons correction). There was no significant difference in the performance of single-unit and multi-unit features selected using PCA and MIM (Two sample t-test, $p < 0.05$). Whereas, single-unit features selected using Wilcoxon signed-rank test and Relative Importance performed significantly better than the multi-unit features selected using the respective algorithms.

Robustness to Simulated Failure

There was a total of 96 multi-unit features and 350 single-unit features from neural data recorded from post-implantation day 36 available for this analysis (corresponding to 100% of features). Therefore, for the 10% case there was 9 multi-unit features and 35 single-unit features. There is a general trend of decrease in the performance of feature selection algorithms when we decrease the number of features from 100 to 10%. While using multi-unit firing rate, the performance of PCA was best at 64.82 $\pm$ 2.27% for 10% of multi-unit features, whereas the performance of Wilcoxon signed-rank test was 21.08 $\pm$ 0.63%. When we used single-unit firing rate as the feature vector, the robustness to simulated failure was higher for all feature selection algorithms when compared to their respective multi-unit firing rate. In case of Wilcoxon signed-rank test there was a ∼10% increase in classification accuracy while there was a ∼40% increase in classification accuracy for MIM based feature selection. The performance of MIM feature selection for single-unit firing rate stayed above 90% classification accuracy even while using only 10% of the available units. MIM based single-unit features performed significantly better than all of the other algorithms for all levels of simulated failure (100–10%) (Kruskal-Wallis test, $p < 0.05$).

Longevity of Neural Decodes

The improvement in classification accuracy from multi-unit to single-unit firing rate requires an AP isolating pre-processing procedure. Relative importance, PCA and MIM had comparable accuracies across 47 sessions and performed better than randomly selected features (**Figures 12**, **13**).

Assessing the chronic decoding capability of various feature selection methods, MIM produced the best results for both single-unit and multi-unit based firing rate (**Table 2**). The

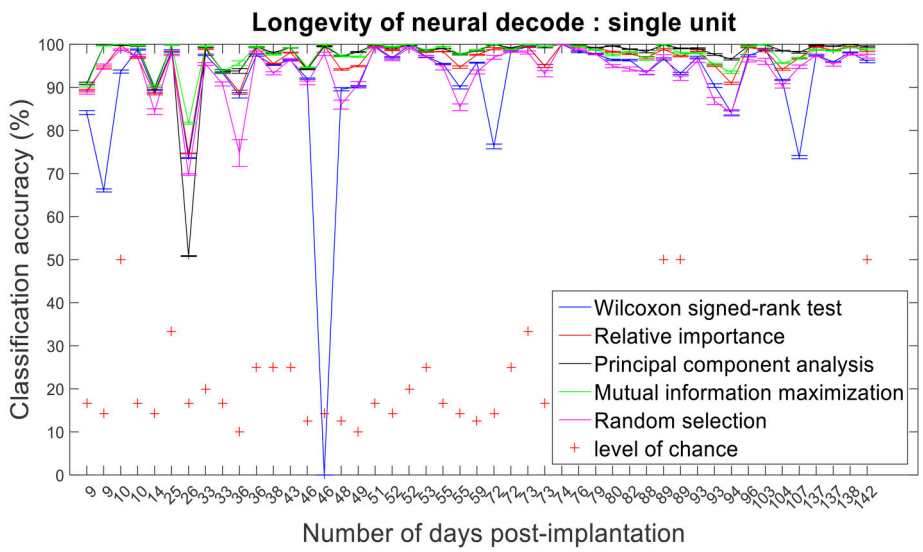

FIGURE 13 | Longevity of neural decodes using single-unit firing rate. The optimal number of features for each feature selection technique was identified using an iterative cross validation scheme. For a given day, cross validation and performance evaluation were computed as described in section Performance Metrics.

TABLE 2 | Longevity of neural decoding.

	Wilcoxon signed-rank test	Relative importance	Principal component analysis	Random selection
Multi-unit	46	21	13	45
Single-unit	45	32	13	45

The values in this table correspond to the number of sessions during which MIM yielded higher decoding accuracies compared to the other methods.

decoding accuracies of MIM based feature selection was compared to the other methods used in this analysis (two sample t-test, $p < 0.05$, α – values calculated using Bonferroni correction to account for multiple comparisons correction). In general, single-unit firing rate feature vector yielded slightly better (∼3–4% on average) performance compared to multi-unit firing rate feature vector for all feature selection methods except Wilcoxon signed-rank test. The chronic decoding results also validate the viability of using a neuroprosthetic device with high classification accuracies (>90% classification accuracy on average).

Isolating the APs from individual neurons is routinely performed on neural recordings from microelectrodes. We have shown that by applying feature selection techniques to single-unit and multi-unit firing rates, we can get comparable performance over a chronic level. However, utilizing single-unit firing rates demonstrated better performance than multi-unit firing rates when the number of active electrodes decreased.

DISCUSSION

Feature selection is an efficient method to cope with the "curse of dimensionality." As explained in the previous sections, performing feature selection increases the amount of data that is bounded by the mean ± 1 standard deviation region. Reducing the dimensionality of neural data from a few hundred features to an average of 20 features, increases the amount of data bounded by the mean ± 1 standard deviation region exponentially. Therefore, the sparsity of data points in the feature space is reduced. In addition to reducing the sparsity, feature selection algorithms also inundate the feature space with more relevant information based on some criteria (Guyon and Elisseeff, 2003). In a way, feature selection can be thought of as a procedure to "prune" the feature space with only "informative" features. All the feature selection algorithms consistently performed better than the randomly selected features. This significant improvement in performance adds ∼10% accuracy in case of both multi-unit and single-unit features compared to randomly selected features. Ideally in real world applications, we would expect the prosthesis to work with 100% accuracy for all different types of movement. To increase user compliance and ease of use, feature selection algorithms must yield accuracies as close to 100% as possible. Misclassifications in prediction can impede or in the worst-case cause physical damage to the user and/or people around them. Misclassifications in real time prediction can lead to undamaging mishaps that might still be critical in accomplishing tasks such as slips while holding a cup of coffee or other objects that might steer the user away from efficiently using the prosthesis for activities of daily living. We also speculate that with increasing misclassifications, user acceptance and performance might deteriorate non-linearly.

Feature selection algorithms operate in various mechanisms and perform significantly better than level of chance and randomly selected features. While Wilcoxon signed-rank test, Relative Importance and MIM retain the innate properties of the feature space (in terms of retaining it in time domain), PCA transforms the features to uncorrelated, orthogonally located principal component axes. It is interesting to note that for many sessions, PCA has comparable performance as MIM. Exploiting this property of PCA and the noise reduction it provides innately, it will be interesting to program algorithms that do not require re-training for each session. This would be a significant improvement in terms of user experience since training time is usually of the order of 20–30 min (performing the training trials and parameter selection for the feature selection and machine learning algorithm) which might be monotonous and tiresome.

Global models, i.e., models that are trained on multiple subjects and then tested on data from an unseen test subject are used for categorizing subjects into groups, e.g., diagnosis. For such an application, a subject-wise cross validation approach is preferred. Subject specific models, i.e., models that are trained on multiple segments of past data and then tested on unseen current data in a single subject are used for estimation of the current state of a given subject, e.g., prognosis. The appropriate approach is needed to approximate the use-case in machine learning (Saeb et al., 2017). We are developing a model that is unique to each subject, therefore, the appropriate method of cross validation is by partitioning the training and testing sets sequentially based on time from an individual subject rather than across multiple subjects. It is also not scientifically accurate to group data from different subjects as the placement of the electrode grids relative to the anatomy of the motor cortex will vary from subject to subject, resulting in a unique spatial sampling of the neurological data from each subject. Using a subject specific approach an intracortical prosthesis allowing people with paralysis to communicate using a virtual keyboard been demonstrated (Pandarinath et al., 2017). We believe that developing subject specific models is the appropriate method for developing BCIs.

One of the limitations of developing subject specific models for clinical applications is the lack of generalization across subjects. The data used in this study was recorded from the primary motor cortex of a healthy NHP. The primary motor cortex is a relatively well-understood part of the brain where the firing of APs is correlated and causally related to movement. The somatotopic and cytoarchitectonic structure of the primary motor cortex is conserved across primates. Therefore, it is a fair assumption that the primary motor cortex of this animal is a standard representation of the primary motor cortex of primates. Although it is impossible to predict the global performance of an algorithmic approach *a priori*, given the conserved structure

of the primary motor cortex, we believe that general trends presented in our analysis will still be transferable across subjects and to similar neuroprosthetic applications.

In this study, we have tested the feature selection algorithms based on scenarios encountered with real-world neural data. Loss of active single and multi-units over a long duration of time has been observed and reported in various studies. In order to make a neuroprosthesis commercially and practically viable, the algorithm must be robust to handle reduction of available features. We have reported the performance of feature selection algorithms when subjected to a reduced subset of features. We achieved accuracies several folds above level of chance with only 10% of the single-unit features using MIM based feature selection. One of the main reasons for the loss of active single and multi-units is due to physiological interactions at the tissue-electrode interface. With technology available at our disposal today, the only way to cope with such physiological interactions might be to replace the micro-electrode array itself. Feature selection algorithms help sustain the performance of the neural decode and maximize the classification accuracy when encountering such intractable conditions.

During some chronic microelectrode array implantations, several studies have reported losing neural information (Frien and Eckhorn, 2000; Leopold and Logothetis, 2003; O'Leary and Hatsopoulos, 2006; Stark and Abeles, 2007; Berens et al., 2008; Jia et al., 2011). In this paper, we compared the performance of multi-units and single-units neural features to simulated failure. Single-unit features were more robust to simulated failure than multi-unit features. We speculate that multi-unit features performed poorer than single-unit features due to aggregation of neural information from the underlying single-units. The amplitude and frequency of firing of the underlying single-units play a significant role in helping decode motor movements. Single-units with unique information could be masked by other single units with higher frequency of firing, therefore, increasing the chance of redundant information when viewing neural information as multi-units. Using single-units might help provide information that results in higher separability of the classes, especially when the number of neural units decreases (like in a simulated failure model).

Neural decoding algorithms must also be reliable over a long duration of time. In this paper, we also present results of various feature selection algorithms over 47 sessions of neural decode. Across all the sessions, single-unit and multi-unit features had comparable performances for multiple types of movements. According to our results, for 60% of the sessions there was a significant difference between the performance of single and multi-unit features. Although there is an average ∼5% increase in performance when using single-unit features, it comes with a trade-off of expensive computation. This computational latency can also manifest in the form of execution delays of the neuroprosthesis while performing a task which might directly affect user performance. We speculate that MIM performs better across all three performance metrics as it maximizes the class conditional entropies of features in the predictor space. Future analysis will investigate the stability of neural decodes. Stability of neural decodes refers to the performance of a trained model over time without updating the model. The stability of neural decoding models will impact how often a user will need to retrain the classifier model.

ETHICS STATEMENT

This study was carried out in accordance with the recommendations of IACUC. The protocol was approved by the University of Utah.

AUTHOR CONTRIBUTIONS

SP and BG designed the methodology, performed the analysis and wrote the manuscript. JB and BG designed and performed the experiments and collected data used in this analysis. BG is the senior author.

ACKNOWLEDGMENTS

This research was supported by CDMRP W81XWH-14-1-0456, DARPA N66001-12-C-4042, and ASU-Mayo Seed Grant. Results included in this paper were presented as part of Master's thesis at Arizona State University (Padmanaban, 2015)

REFERENCES

Aflalo, T., Kellis, S., Klaes, C., Lee, B., Shi, Y., Pejsa, K., et al. (2015). Neurophysiology. Decoding motor imagery from the posterior parietal cortex of a tetraplegic human. *Science* 348, 906–910. doi: 10.1126/science.aaa5417

Baker, J., Bishop, W., Kellis, S., Levy, T., House, P., and Greger, B. (2009). "Multi-scale recordings for neuroprosthetic control of finger movements," in *Engineering in Medicine and Biology Society, 2009. EMBC 2009. Annual International Conference of the IEEE*, 4573–4577.

Bashashati, A., Fatourechi, M., Ward, R. K., and Birch, G. E. (2007). A survey of signal processing algorithms in brain–computer interfaces based on electrical brain signals. *J. Neural Eng.* 4, R32–R57. doi: 10.1088/1741-2560/4/2/R03

Berens, P., Keliris, G. A., Ecker, A. S., Logothetis, N. K., and Tolias, A. S. (2008). Comparing the feature selectivity of the gamma-band of the local field potential and the underlying spiking activity in primate visual cortex. *Front. Syst. Neurosci.* 2:2. doi: 10.3389/neuro.06.002.2008

Bitzer, S., and van der Smagt, P. (2006). "Learning EMG control of a robotic hand: towards active prostheses," in *Robotics and Automation, 2006. ICRA 2006. Proceedings 2006 IEEE International Conference*, 2819–2823.

Brown, G., Pocock, A., Zhao, M., and Luján, M. (2012). Conditional likelihood maximisation: a unifying framework for information theoretic feature selection. *J. Mach. Learn. Res.* 13, 27–66.

Carmena, J. M., Lebedev, M. A., Crist, R. E., O'doherty, J. E., Santucci, D. M., Dimitrov, D. F., et al. (2003). Learning to control a brain-machine interface for reaching and grasping by primates. *PLoS Biol.* 1:E42. doi: 10.1371/journal.pbio.0000042

Collinger, J. L., Wodlinger, B., Downey, J. E., Wang, W., Tyler-Kabara, E. C., Weber, D. J., et al. (2013). High-performance neuroprosthetic control by an individual with tetraplegia. *Lancet* 381, 557–564. doi: 10.1016/S0140-g36(12)61816-9

Demirer, R. M., Ozerdem, M. S., and Bayrak, C. (2009). Classification of imaginary movements in ECoG with a hybrid approach based on multi-dimensional hilbert-SVM solution. *J. Neurosci. Methods* 178, 214–218. doi: 10.1016/j.jneumeth.2008.11.011

Duan, K., and Keerthi, S. S. (2005). "Which is the best multiclass SVM method? An empirical study," in *Multiple Classifier Systems* (Springer), 278–285.

Ethier, C., Oby, E. R., Bauman, M., and Miller, L. E. (2012). Restoration of grasp following paralysis through brain-controlled stimulation of muscles. *Nature* 485, 368–371. doi: 10.1038/nature10987

Frien, A., and Eckhorn, R. (2000). Functional coupling shows stronger stimulus dependency for fast oscillations than for low-frequency components in striate cortex of awake monkey. *Eur. J. Neurosci.* 12, 1466–1478. doi: 10.1046/j.1460-9568.2000.00026.x

Ganguly, K., and Carmena, J. M. (2009). Emergence of a stable cortical map for neuroprosthetic control. *PLoS Biol.* 7:e1000153. doi: 10.1371/journal.pbio.1000153

Garrett, D., Peterson, D. A., Anderson, C. W., and Thaut, M. H. (2003). Comparison of linear, nonlinear, and feature selection methods for EEG signal classification. *IEEE Trans. Neural. Syst. Rehabil. Eng.* 11, 141–144. doi: 10.1109/TNSRE.2003.814441

Gilja, V., Nuyujukian, P., Chestek, C. A., Cunningham, J. P., Byron, M. Y., Fan, J. M., et al. (2012). A high-performance neural prosthesis enabled by control algorithm design. *Nat. Neurosci.* 15, 1752–1757. doi: 10.1038/nn.3265

Gilja, V., Pandarinath, C., Blabe, C. H., Nuyujukian, P., Simeral, J. D., Sarma, A. A., et al. (2015). Clinical translation of a high-performance neural prosthesis. *Nat. Med.* 21, 1142–1145. doi: 10.1038/nm.3953

Guyon, I., and Elisseeff, A. (2003). An introduction to variable and feature selection. *J. Mach. Learn. Res.* 3, 1157–1182. doi: 10.1162/153244303322753616

Hochberg, L. R., Serruya, M. D., Friehs, G. M., Mukand, J. A., Saleh, M., Caplan, A. H., et al. (2006). Neuronal ensemble control of prosthetic devices by a human with tetraplegia. *Nature* 442, 164–171. doi: 10.1038/nature04970

House, P. A., MacDonald, J. D., Tresco, P. A., and Normann, R. A. (2006). Acute microelectrode array implantation into human neocortex: preliminary technique and histological considerations. *Neurosurg. Focus* 20, 1–4. doi: 10.3171/foc.2006.20.5.5

Hsu, C., and Lin, C. (2002). A comparison of methods for multiclass support vector machines. *IEEE Trans. Neural. Netw.* 13, 415–425. doi: 10.1109/72.991427

Hwang, E. J., and Andersen, R. A. (2013). The utility of multichannel local field potentials for brain–machine interfaces. *J. Neural. Eng.* 10:046005. doi: 10.1088/1741-2560/10/4/046005

Jia, X., Smith, M. A., and Kohn, A. (2011). Stimulus selectivity and spatial coherence of gamma components of the local field potential. J. *Neurosci.* 31, 9390–9403. doi: 10.1523/JNEUROSCI.0645-11.2011

Jolliffe, I. (2002). *Principal Component Analysis*. Wiley Online Library.

Kantardzic, M. (2011). *Data mining: Concepts, Models, Methods, and Algorithms*. John Wiley & Sons.

Kellis, S., Miller, K., Thomson, K., Brown, R., House, P., and Greger, B. (2010). Decoding spoken words using local field potentials recorded from the cortical surface. *J. Neural Eng.* 7:056007. doi: 10.1088/1741-2560/7/5/056007

Kim, H., Kim, Y., Shin, H., Aggarwal, V., Schieber, M. H., and Thakor, N. V. (2012). Neuron selection by relative importance for neural decoding of dexterous finger prosthesis control application. *Biomed. Signal. Process. Control.* 7, 632–639. doi: 10.1016/j.bspc.2012.03.003

Kim, S., Simeral, J. D., Hochberg, L. R., Donoghue, J. P., and Black, M. J. (2008). Neural control of computer cursor velocity by decoding motor cortical spiking activity in humans with tetraplegia. *J. Neural. Eng.* 5, 455–476. doi: 10.1088/1741-2560/5/4/010

Kohavi, R., and John, G. H. (1997). Wrappers for feature subset selection. *Artif. Intell.* 97, 273–324. doi: 10.1016/S0004-3702(97)00043-X

Kubánek, J., Miller, K., Ojemann, J., Wolpaw, J., and Schalk, G. (2009). Decoding flexion of individual fingers using electrocorticographic signals in humans. *J. Neural. Eng.* 6:066001. doi: 10.1088/1741-2560/6/6/066001

Leopold, D. A., and Logothetis, N. K. (2003). Spatial patterns of spontaneous local field activity in the monkey visual cortex. *Rev. Neurosci.* 14, 195–205. doi: 10.1515/REVNEURO.2003.14.1-2.195

Lewicki, M. S. (1998). A review of methods for spike sorting: the detection and classification of neural action potentials. *Network* 9, R53–R78. doi: 10.1088/0954-898X_9_4_001

Little, M. A., Varoquaux, G., Saeb, S., Lonini, L., Jayaraman, A., Mohr, D. C., et al. (2017). Using and understanding cross-validation strategies. Perspectives on Saeb et al. *Gigascience* 6, 1–6. doi: 10.1093/gigascience/gix020

Lu, Y., Cohen, I., Zhou, X. S., and Tian, Q. (2007). "Feature selection using principal feature analysis," in *Proceedings of the 15th International Conference on Multimedia*, 301–304.

Musallam, S., Corneil, B. D., Greger, B., Scherberger, H., and Andersen, R. A. (2004). Cognitive control signals for neural prosthetics. *Science* 305, 258–262. doi: 10.1126/science.1097938

O'Leary, J. G., and Hatsopoulos, N. G. (2006). Early visuomotor representations revealed from evoked local field potentials in motor and premotor cortical areas. *J. Neurophysiol.* 96, 1492–1506. doi: 10.1152/jn.00106.2006

Padmanaban, S. (2015). *Comparison of Feature Selection Methods for Robust Dexterous Decoding of Finger Movements from the Primary Motor Cortex of a Non-Human Primate using Support Vector Machine*.

Pandarinath, C., Nuyujukian, P., Blabe, C. H., Sorice, B. L., Saab, J., Willett, F. R., et al. (2017). High performance communication by people with paralysis using an intracortical brain-computer interface. *Elife* 6:e18554. doi: 10.7554/eLife.18554

Platt, J. (1999). "Fast training of support vector machines using sequential minimal optimization," in *Advances in Kernel Methods—Support Vector Learning*, 3.

Quandt, F., Reichert, C., Hinrichs, H., Heinze, H., Knight, R., and Rieger, J. W. (2012). Single trial discrimination of individual finger movements on one hand: a combined MEG and EEG study. *Neuroimage* 59, 3316–3324. doi: 10.1016/j.neuroimage.2011.11.053

Randles, R. H. (1988). *Wilcoxon Signed Rank Test. Encyclopedia of Statistical Sciences*

Saeb, S., Lonini, L., Jayaraman, A., Mohr, D. C., and Kording, K. P. (2017). The need to approximate the use-case in clinical machine learning. *Gigascience* 6, 1–9. doi: 10.1093/gigascience/gix019

Santhanam, G., Ryu, S. I., Byron, M. Y., Afshar, A., and Shenoy, K. V. (2006). A high-performance brain–computer interface. *Nature* 442, 195–198. doi: 10.1038/nature04968

Shenoy, K. V., Meeker, D., Cao, S., Kureshi, S. A., Pesaran, B., Buneo, C. A., et al. (2003). Neural prosthetic control signals from plan activity. *Neuroreport* 14, 591–596. doi: 10.1097/00001756-200303240-00013

Shenoy, P., Miller, K. J., Ojemann, J. G., and Rao, R. P. (2007). "Finger movement classification for an electrocorticographic BCI," in *Neural Engineering, 2007. CNE'07. 3rd International IEEE/EMBS Conference* 192–195.

Shoham, S., Fellows, M. R., and Normann, R. A. (2003). Robust, automatic spike sorting using mixtures of multivariate t-distributions. *J. Neurosci. Methods* 127, 111–122. doi: 10.1016/S0165-0270(03)00120-1

Stark, E., and Abeles, M. (2007). Predicting movement from multiunit activity. *J. Neurosci.* 27, 8387–8394. doi: 10.1523/JNEUROSCI.1321-07.2007

Torkkola, K. (2003). Feature extraction by non parametric mutual information maximization. *J. Mach. Learn. Res.* 3, 1415–1438.

Truccolo, W., Eden, U. T., Fellows, M. R., Donoghue, J. P., and Brown, E. N. (2005). A point process framework for relating neural spiking activity to spiking history, neural ensemble, and extrinsic covariate effects. *J. Neurophysiol.* 93, 1074–1089. doi: 10.1152/jn.00697.2004

Vetter, R. J., Williams, J. C., Hetke, J. F., Nunamaker, E., and Kipke, D. R. (2004). Chronic neural recording using silicon-substrate microelectrode arrays implanted in cerebral cortex. *IEEE Trans. Biomed. Eng.* 51, 896–904. doi: 10.1109/TBME.2004.826680

Wang, B., Shi, W., and Miao, Z. (2015). Confidence analysis of standard deviational ellipse and its extension into higher dimensional euclidean space. *PLoS ONE* 10:e0118537. doi: 10.1371/journal.pone.0118537

Wang, W., Degenhart, A. D., Collinger, J. L., Vinjamuri, R., Sudre, G. P., Adelson, P. D., et al. (2009). "Human motor cortical activity recorded with micro-ECoG electrodes, during individual finger movements," in *Engineering in Medicine and Biology Society, 2009. EMBC 2009. Annual International Conference of the IEEE,* 586–589.

Wissel, T., Pfeiffer, T., Frysch, R., Knight, R. T., Chang, E. F., Hinrichs, H., et al. (2013). Hidden markov model and support vector machine based decoding of finger movements using electrocorticography. *J. Neural Eng.* 10:056020. doi: 10.1088/1741-2560/10/5/056020

Conflict of Interest Statement: The authors declare that the research was conducted in the absence of any commercial or financial relationships that could be construed as a potential conflict of interest.

IOP Publishing Journal of Neural Engineering
J. Neural Eng. 13 (2016) 036001 (15pp) doi:10.1088/1741-2560/13/3/036001

Restoring motor control and sensory feedback in people with upper extremity amputations using arrays of 96 microelectrodes implanted in the median and ulnar nerves

T S Davis[1,2,5], H A C Wark[1,5], D T Hutchinson[3], D J Warren[1], K O'Neill[1], T Scheinblum[1], G A Clark[1], R A Normann[1] and B Greger[1,4]

[1] Department of Bioengineering, University of Utah, Salt Lake City, UT 84112, USA
[2] Department of Neurosurgery, University of Utah, Salt Lake City, UT 84132, USA
[3] Department of Orthopaedics, University of Utah, Salt Lake City, UT 84108, USA
[4] School of Biological & Health Systems Engineering, Arizona State University, Tempe, AZ 85287, USA

E-mail: bradley.greger@asu.edu

Received 6 March 2014, revised 8 December 2015
Accepted for publication 10 February 2016
Published 22 March 2016

Abstract

Objective. An important goal of neuroprosthetic research is to establish bidirectional communication between the user and new prosthetic limbs that are capable of controlling >20 different movements. One strategy for achieving this goal is to interface the prosthetic limb directly with efferent and afferent fibres in the peripheral nervous system using an array of intrafascicular microelectrodes. This approach would provide access to a large number of independent neural pathways for controlling high degree-of-freedom prosthetic limbs, as well as evoking multiple-complex sensory percepts. *Approach*. Utah Slanted Electrode Arrays (USEAs, 96 recording/stimulating electrodes) were implanted for 30 days into the median (Subject 1-M, 31 years post-amputation) or ulnar (Subject 2-U, 1.5 years post-amputation) nerves of two amputees. Neural activity was recorded during intended movements of the subject's phantom fingers and a linear Kalman filter was used to decode the neural data. Microelectrode stimulation of varying amplitudes and frequencies was delivered via single or multiple electrodes to investigate the number, size and quality of sensory percepts that could be evoked. Device performance over time was assessed by measuring: electrode impedances, signal-to-noise ratios (SNRs), stimulation thresholds, number and stability of evoked percepts. *Main results*. The subjects were able to proportionally, control individual fingers of a virtual robotic hand, with 13 different movements decoded offline ($r = 0.48$) and two movements decoded online. Electrical stimulation across one USEA evoked >80 sensory percepts. Varying the stimulation parameters modulated percept quality. Devices remained intrafascicularly implanted for the duration of the study with no significant changes in the SNRs or percept thresholds. *Significance*. This study demonstrated that an array of 96 microelectrodes can be implanted into the human peripheral nervous system for up to 1 month durations. Such an array could provide intuitive control of a virtual prosthetic hand with broad sensory feedback.

S Online supplementary data available from stacks.iop.org/JNE/13/036001/mmedia

[5] These authors contributed equally to this work.

Keywords: neural prosthesis, peripheral nerve interface, brain machine interface

(Some figures may appear in colour only in the online journal)

1. Introduction

The volitional control of movement involves a complex and integrated hierarchy of sensory-motor neural systems. Arrays of microelectrodes implanted at various levels in this hierarchy have been used to record spatiotemporal patterns of neural activity and for correlation of these patterns with sensory stimulation and motor behaviors. Early efforts to obtain volitional control signals from the nervous system were conducted in non-human primates by decoding neural activity patterns recorded with microelectrodes implanted in the motor cortex [1–6]. Researchers have been translating these efforts to human subjects. Severely paralyzed patients have had electrode arrays implanted into areas of the cerebral cortex involved in motor control. Using these electrode arrays electrophysiological recordings of action potential firing from neurons have provided control over external devices ranging from two-dimensional movements of computer cursors to 10 degrees-of-freedom (DOF) robotic arms and hands [7–16]. Investigations of electrode arrays that rest on the surface of the cerebral cortex, i.e. electrocorticography and micro-electrocorticography, have been perform in patients undergoing neural surgery for the treatment of epilepsy. These surface electrodes record the aggregate signals from groups of neurons, rather than from individual neurons, but are still capable of providing control signals for prosthetic devices [17–31]. In these studies the subjects relied on visual or auditory sensory input to provide feedback of their performance, and ongoing research is investigating using central nervous system stimulation to provide feedback from prosthetic limbs [32, 33]. The central nervous system is an effective implantation site for people with paralysis, however investigations of utilizing peripheral nerve approaches such as targeted reinnervation [34, 35] or peripheral nerve electrode implantation [36–45] are warranted for people with amputations.

The current state-of-the-art for people with upper-limb amputations are mechanically or myoelectrically controlled prosthetic arms with few DOF that do not provide sensory feedback [46]. Next generation prosthetic arms are being developed with upwards of 26 DOF [47, 48] and with embedded sensors intended to be used to provide sensory feedback to the user [37, 44, 49]. Several strategies are being investigated for providing sensory feedback from these new prosthetic limbs including surface vibrators [49], and extraneural [41, 42, 45, 50] or intraneural [44, 51–54] electrodes. The number of extra/intraneural electrodes (or 'contacts') implanted into each human peripheral nerve has been increasing, with previous studies having used: one [37, 40], six [55], eight [45, 56], sixteen [44], or twenty [53] electrodes to established bidirectional communication with a subject's peripheral nervous system.

Modern, high-DOF bidirectional prosthetic arms and hands may require numerous microelectrodes to obtain sufficiently independent control and feedback signals. Motor intent has been decoded online and offline [37, 43, 44, 55] with control of up to three different movements from offline decodes [37, 43, 44], and sensory feedback has been provided via electrical stimulation [37, 38, 40, 44, 45, 49, 56, 57] with the evocation of a maximum of nine different percepts for a single neural implant [44].

We report herein an approach for the control of prosthetic limbs using an array of 96 microelectrodes, the Utah Slanted Electrode Array (USEA) [52], which increases the number of electrodes that have been used to interface with a peripheral nerve by 80 more electrodes per nerve over previously investigated neural interfaces [44, 45]. This work was conducted in two subjects who had previously undergone transradial amputations. Each subject had a microelectrode array implanted in one of their transected peripheral nerves in order to selectively access individual or small groups of motor and/or sensory fibres. Selective spatiotemporal neural activity patterns were recorded when subjects were asked to make volitional movements of their phantom fingers. Closed-loop neural control of multiple cursors or virtual robotic fingers was achieved in each subject with two DOF control achieved online for both subjects.

Electrophysiological recordings from, and electrical stimulation of, peripheral nerves using transversal multichannel intrafascicular electrodes have enable human subjects to make three different grasp movements utilizing sensory feedback provided by sensors in a prosthetic hand [43, 44]. Up to eight sensory percept were evoked using long-term implanted peripheral nerve cuff electrodes that did not penetrate the nerve [45]. We investigated electrophysiological recordings from, and stimulation of, human peripheral nerves with high-count (96 electrodes) intrafascicular electrodes. Utilizing this device we show that up to 13 different movements can be decoded from human peripheral nerve signals using visual feedback of movements. Additionally, we show that up to 86 percepts (number of percepts in a single stimulation session) with an average of 81 percepts over the study duration can be evoked. Together these studies demonstrate that an array of electrodes interfacing with residual nerves of patients with a forearm amputation allow for selective access of both sensory and motor nerve fibres. These results further suggest that intuitive and dexterous control of prosthetic fingers with sensory feedback can be provided for future bidirectional prosthetic limbs using an array of intrafascicularly and perifascicularly implanted microelectrodes.

2. Methods

This study was approved by the University of Utah Institutional Review Board, the Salt Lake City Veterans Affairs Hospital Research and Development Service Center and the US Federal Defense Advanced Research Projects Agency.

2.1. Pre-study enrolment period

Two volunteers with previous transradial amputations participated in this study and underwent implantation for a one month period with a USEA into their median nerve (Subject 1-M, Median nerve implant, 31 years post-amputation) or ulnar nerve (Subject 2-U, Ulnar nerve implant, 1.5 years post-amputation). Potential volunteers were evaluated for the extent by which they perceived that they were able to make specific movements with their phantom fingers. The duration, frequency, and intensity of phantom limb sensations, including pain, were documented in the patient's journal throughout the study. Multiple phantom movements mediated by median and ulnar nerve activity were evaluated in each volunteer, and the extent of their ability to move their fingers was noted from their descriptions (e.g. Subject 1-M had 'a very fluid hand' but Subject 2-U's phantom fingers were often 'clenched tight'). After selection for inclusion in the study, volunteers were then given a mirror box and specific exercises to perform in order to strengthen their perceived ability to move the digits on their phantom hands. Volunteers were asked to document any changes in the perceived control of their phantom hand, and if any decreased control or unpleasant sensation was experienced, the volunteers would have been asked to discontinue use of the mirror box (none of the volunteers experienced such changes). Prior to enrolment, volunteers underwent a psychosocial evaluation in order to determine if any underlying psychological conditions were present which would have excluded them from the study.

2.2. Nerve electrode arrays

The USEA (Blackrock Microsystems, Salt Lake City, UT, USA) has been described elsewhere [52] and will only be briefly described herein. The array consists of 100 electrodes (96 recording/stimulating electrodes, 4 electrodes wired as unused backup reference electrode) with lengths ranging from 0.5 to 1.5 mm (10 by 10 grid with 400 μm spacing) that project out from a $4 \times 4 \times 0.3\,\mathrm{mm}^3$ substrate. Lead wire lengths from the connector (custom-built item compatible with the ZIF Clip 96, Tucker Davis Technologies, Inc., Alachua, FL, USA) to the array were configured for implantation into the upper limb nerves at a transradial location. Lead wires included: (1) 100 lead wires (~9 cm long) with 96 of the wires bonded to electrodes used for recording and 4 bonded to backup reference electrodes, (2) two low-impedance platinum reference wires (~8.5 cm long) connected to the reference channel, and (3) two low-impedance platinum ground wires (~7.5 cm long) connected to the recording amplifier ground and stimulation return. Approximately 10 mm of the distal ends of the reference and ground wires were twisted and looped back, with distal ends secured onto the proximal reference or ground wires by coating with silicone (MED-4211, NuSil Technology LLC, Carpinteria, CA, USA). Thus, each loop consisted of two wires (two reference or two ground wires), and the distal ends of these loops were de-insulated to reduce their impedance. The lengths of the reference and ground wires were measured from the base of the connector to the end of the distal loop. The reference and ground wires were placed inside the nerve wrap (see section 2.3 surgical procedures) near the electrode array.

A Neuroport data acquisition system (Blackrock Microsystems, Salt Lake City, UT, USA) was used to measure the electrode impedances. A sinusoidal current at 1 kHz was passed through a reference electrode, and impedance was simultaneously computed on all electrodes. Before implantation, the electrodes on each device had an average (mean $\pm$ std) impedance of $75 \pm 57\,\mathrm{k}\Omega$ (Subject 1-M) and $90 \pm 28\,\mathrm{k}\Omega$ (Subject 2-U). Working electrodes were defined as electrodes with an impedance $<500\,\mathrm{k}\Omega$.

2.3. Surgical procedures

The distal nerve end was exposed and the implant site was selected such that it was distal to any branching points and proximal to the transitional zone adjacent to the neuroma (approximately 5–10 mm from the neuroma). The USEA was then passed transcutaneously via a trocar (7–8 mm diameter) down to the exposed implantation site. A metal platform was placed underneath the nerve, along with a high visibility background and a reconstituted organic nerve wrap (AxoGuard Nerve Wrap, AxoGen Inc., Alachua, FL, USA). The lead wires were then sutured (8-0 nylon) to the epineurium (~5 mm from the base of the electrode array). The USEAs were inserted with a pneumatic insertion device [31] that was hand-held by the surgeon. The implanted USEA, reference wires, ground wires, and nerve were contained within the organic nerve wrap, which was closed snuggly around the implant site with titanium vascular clips (supplementary figure 1). The organic nerve wrap was sutured (8-0 nylon) to the epineurium proximal and distal to the array site to prevent movement of the wrap along the nerve.

The percutaneous site was dressed with a 1″ diameter, clorohexadine antibacterial patch (Biopatch, Ethicon Inc., Johnson & Johnson, New Brunswick, NJ, USA). In Subject 2-U, the connector was sutured down to the skin to prevent stress on the lead wires due to movement of the connector. The entire percutaneous site was layered with gauze and covered with a breathable and waterproof transparent dressing (Tegaderm, 3M Healthcare, St. Paul MN, USA). The gauze and film dressing was changed during each experimental session and antibacterial patches were replaced every 7–10 days. To decrease the inflammatory process and potentially assist in enhanced signal quality over time, subjects were given dexamethasone ($0.1\,\mathrm{mg\,kg}^{-1}$ IV, Mylan Institutional LLC, Rockford, IL) intraoperatively after removal of the tourniquet and minocycline (100 mg BID, Watson Pharmaceuticals, Parsippany, NJ) 2 days prior and for 5 days after surgery [58, 59].

At the end of the one month experimental period, each subject underwent explantation of the USEAs under general anaesthesia. The percutaneous wires were cut at the level of the skin and the entire limb was then prepared for surgery. The implant side was exposed and the lead, reference, and ground wires were cut adjacent to the organic nerve wrap

containment system and all wires were removed. The entire implant site and neuroma was excised. The new nerve end was then sutured deep in the surrounding musculature according to standard surgical procedures for neuroma excisions.

2.4. Experimental sessions

Two hour experimental sessions were performed on an average of three times per week. The time was limited by subject availability or their willingness to continue testing (Subject 1-M underwent 12 total experimental sessions: 6 electrophysiological recording sessions and 8 microstimulation sessions; Subject 2-U underwent a total of 14 experimental sessions: 13 electrophysiological recording sessions and 8 microstimulation sessions). All experimental sessions were recorded with a video camera, which was time-stamped to the neural recording or stimulation data.

2.5. Neural recordings, decoding and instrumentation

Neural signals were amplified and recorded using active headstage cables (ZIF-Clip 96, Tucker Davis Technologies, Inc., Alachua, FL, USA) that connected to a custom-built interconnect board used to interface the ZIF-Clip cable with the Neuroport data acquisition system. The continuous neural signals were band-pass filtered with cutoff frequencies of 0.3 Hz (1st-order high-pass Butterworth filter) and 7500 Hz (3rd-order low-pass Butterworth filter) and sampled at 30 kHz. Online multi-unit activity was extracted from high-pass filtered recording data (250 Hz 4th-order Butterworth filter) by setting a threshold using the auto threshold setting in the Neuroport data acquisition software (multiplier = 3, threshold = multiplier × noise estimate of the signal). For each of the 96 neural recording channels, multi-unit neural firing rates were calculated using unsorted spikes and a moving box-car average of 300 ms with an update period of 33 ms. Offline, action potentials were isolated from the high-pass filtered data using commercially available software (Offline Sorter version 3, Plexon Inc., Dallas, Texas, USA). Signal-to-noise ratios (SNRs) were calculated by dividing the mean peak-to-peak action potential amplitude by two times the standard deviation of the recorded noise [60].

2.5.1. Decoding neural signals and control of virtual robotic fingers or computer indicators. A standard Kalman filter was implemented to perform the continuous neural decodes [61]. This algorithm assumes a linear relationship between the kinematics (finger position) and the neural data. For this study, it was used to provide continuous estimates of finger position based on the firing rates of multiple neurons. Sessions began by cueing the subjects to perform multiple flexions, extensions or abductions of their individual phantom fingers. A total of 4 movements were performed for Subject 1-M (Thumb-Flex, Index-Flex, Middle-Flex, and Ring-Flex) and 13 movements for Subject 2-U (Thumb-Flex, Thumb-Extend, Index-Flex, Index-Extend, Index-Abduct, Middle-Flex, Middle-Extend, Ring-Flex, Ring-Extend, Ring-Abduct, Little-Flex, Little-Extend, Little-Abduct). These movements are given acronyms based on the first one or two letters of each word, which are used in subsequent figures (e.g., Thumb-Flex = TF). The subjects were instructed to make finger movements by either a computer controlled display of indicators (Subject 1-M) or by movement of virtual robotic fingers [62] (Subject 2-U) (supplementary figure 1). Subject 1-M held a small manipulandum consisting of individual, movable pads that could be depressed by each finger with the subject's intact hand. For Subject 1-M finger position targets were provided on a computer monitor. In order to have a metric of the finger positions of the phantom hand, Subject 1-M was asked to mirror the movements made with their phantom fingers by pressing on the pads of a manipulandum with their intact fingers. During algorithm training for Subject 1-M the finger position of the phantom hand (instruction variable) was measured as the continuous voltage signal from pressure sensors on the pads of the manipulandum, which was displayed by a graphical indicator on the computer monitor. For Subject 2-U the instructions on what finger movements to make were provided using the virtual prosthetic hand. During algorithm training the virtual prosthetic hand made specific finger movements under computer control and Subject 2-U was asked to mimic these movements with their phantom hand. The computer generated positions of the virtual prosthetic fingers (instruction variable) was generated using a cosine function, which was normalized from −1 (full extension/adduction) to +1 (full flexion/abduction). Multi-unit firing rates from selected electrodes and the movement instruction variables were then used to train and test the decode algorithm for both online and offline control.

2.5.2. Online neural decodes. For online decoding, electrodes were selected based on their ability to record movement-correlated action potentials. This selection process was made using two methods: (1) the experimenters viewed a map of correlation coefficients between the instruction variables and the firing rates on each electrode and (2) the experimenters' subjective observations of the high-pass filtered neural data on each electrode during the cued movements. Following electrode selection, the decode algorithm was trained on a set of 10 trials for each movement type. For testing, subjects were asked to control a computer display of indicators (Subject 1-M) or virtual prosthetic fingers (Subject 2-U) and acquire targets in a trial-based format.

Subjects began a trial by moving the fingers of their phantom hand to a neutral, hand-at-rest position, which moved those indicators or virtual prosthetic fingers under neural control to the hand-at-rest start position. The indicators and virtual prosthetic fingers not under neural control were set to, and held at, the start position by the computer. After a few hundred milliseconds, one or more of the computer generated the targets would change spatial location and the subjects were required to match finger positions of all prosthetic fingers under neural control to the new positions of the computer generated targets for at least 300 ms and up to

3000 ms. Targets were presented of varying diameters (30%–36% of full-range movement) and distances (40%–100% of full-range movement) from the starting point. In order to correctly complete a trial, the subjects had to acquire and maintain the tip(s) of the finger(s) of the virtual prosthetic hand under neural control at the target(s). At the completion of a trial the target(s) would return to the hand-at-rest start position and the subjects would have to return the indicators or fingers of the virtual prosthetic hand to the start position in order to begin a new trial. Throughout the trials subjects were instructed to maintain their phantom fingers that were not being instructed to move, i.e. corresponding to the fingers on the virtual prosthetic hand that were not under neural control, at their start positions. This task paradigm assessed the ability of subjects to move the virtual indicator/fingers independently and proportionally. The finger required to move to the target and the position of the target would be changed for different trials. This produced individuated proportional finger movements during simultaneous neural control of multiple fingers (see supplemental video 2).

2.5.3. Offline neural decodes. For offline decoding, an average of 22 (range of 13–37) trials of each movement type recorded during a typical experimental session were analyzed. Electrodes were chosen on the basis of the results of a Wilcoxon signed-rank test. First, a 'baseline-period' was defined as the 2 s period prior to the onset of the movement cue, and a 'movement-period' was defined as the 2 s period after the onset of the cue. Then, the difference in median firing rates was calculated between the 'movement-period' and the 'baseline-period' for all movement types and trials recorded on each electrode. The null hypothesis was that the data came from a continuous, symmetric distribution with a median difference equal to zero (i.e., the electrode did not record increased firing rates in the movement-period compared with the baseline-period). All electrodes for which the null hypothesis was rejected ($p < 0.001$) with a positive median difference from baseline were kept. These electrodes were then sorted in order of increasing median difference and the top 90% of electrodes were used in the offline decode. After electrode selection, the decode algorithm was trained on the first 10 trials for each movement and tested on the remaining 3–27 trials. A Pearson's correlation coefficient (r) between the instruction variable and the Kalman filter estimate of finger positions, calculated for the entire continuous sampling of data corresponding with the trained movements for the remaining 3–27 testing trials, was used to quantify the decode performance.

2.6. Neural stimulation and instrumentation

Current-controlled, biphasic, cathodic-first (without anodic bias) stimulation [63] (IZ2, 128-channel Tucker-Davis Technologies Stimulator, Inc., Alachua, FL, USA) was delivered to individual or subsets of electrodes using custom LabVIEW software (National Instruments Corp., Austin, TX, USA), using the platinum ground wires as a return. The stimulator had a compliance voltage of ± 15 V (LZ48-400, Tucker-Davis Technologies Stimulator, Inc., Alachua, FL, USA). Maximum stimulation was limited by either: (1) the comfort level of the subject, (2) a perceived change in the quality of the percept or (3) if the maximum safety limit for delivering electricity to tissue was reached [64]. The safety limit for injecting charge into the tissue was determined by measuring the maximum cathodic voltage excursion (with a safety limit of -0.6 V) across the electrode and ground during stimulation [65–67]. The voltage drop due to tissue impedance was not subtracted in our calculations, resulting in a conservative estimate of safe stimulation parameters. Stimulation parameters varied depending on the objective of the experimental session. Pulse amplitude, frequency, and train duration ranged from 1 to 100 μA, 1 to 320 Hz, and 0.2 to 60 s, respectively. Pulse width and inter-phase interval were held fixed at 200 μs and 100 μs.

2.6.1. Stimulation across different amplitudes and frequencies (Subject 1-M). In Subject 1-M, stimulation experiments were focused on a subset of electrodes to investigate the subject's ability to detect and discriminate single and multiple sensory percepts and the effects of modulating stimulation frequency on sensory percepts. A custom-built software interface (LabVIEW software, National Instruments Corp., Austin, TX, USA) was used to allow Subject 1-M to control the amplitude of stimulation (1–100 μA in steps of 1 μA) at a constant frequency (200 Hz) and train duration (0.2 s) in order to determine the threshold of a sensory percept (sessions 1–8, post-implantation days 5–26). Control of frequency (1–320 Hz in 1 Hz steps, threshold amplitudes, 0–60 s durations) was provided to the subject by pressing down on a pressure sensor mounted on the manipulandum with a finger from the subject's intact hand (sessions 4–8, post-implantation days 14–26).

2.6.2. Simultaneous multielectrode stimulation (Subject 1-M). Stimulation was delivered via multiple electrodes simultaneously to investigate if the subject could discern multiple electrically evoked percepts simultaneously. Stimulation sessions were performed where the subject was cued that a trial began, but did not know whether stimulation was delivered via either of two electrodes, both electrodes simultaneously, or no-stimulation was delivered. Such blinded-trial data was collected during three different experimental sessions on post-implantation days 13, 19, and 26. Electrodes with different inter-electrode distances were chosen, and supra-threshold stimulation amplitudes were used (day 13—electrodes 16 and 19, 1200 μm distance, 19 μA and 25 μA thresholds; day 19—electrodes 19 and 20, 400 μm distance, 47 μA and 18 μA thresholds; day 26—electrodes 20 and 46, 1442 μm distance, 18 μA and 10 μA thresholds). For each trial, the subject had to record the size, location and intensity of the evoked percept on anterior and/or posterior

maps of a hand. If no percept was evoked, the subject reported no sensation.

2.6.3. Stimulation thresholds for all 96 electrodes over 30 days (*Subject 2-U*). All 96 USEA microelectrodes were individually stimulated (six sessions at 200 Hz on post-implantation days 6–25; two sessions at 20 Hz post-implantation days 26–27) and the threshold, location, size, quality and intensity of each evoked percept was mapped using custom built software (LabVIEW software, National Instruments Corp., Austin, TX, USA). Subject 2-U controlled when stimulation was delivered, but the experimenter controlled the amplitude (1–100 μA in steps of 1–5 μA) and pulse train duration (0.2 or 2 s). The quality of the percept was designated from a list (tingle, pressure, vibration, hot, cold) or could be defined using their own words. When a percept was faint or the subject was unsure of the sensation, stimulation could be repeated until they were sure the percept was electrically evoked (as opposed to a phantom limb sensation).

2.6.4. Stability of percept location over 30 days (*Subject 2-U*). All of the electrodes that evoked a percept during each stimulation session when each electrode in the entire array was stimulated at 200 Hz were analyzed (post-implantation days 10–25; Subject 2-U). A percept was considered stable if it remained in a localized anatomical region of the phantom hand, defined as one of the following: anterior or posterior of a particular finger, the palm, or the back of the hand. If a portion of an evoked percept was located on the border separating two anatomical locations (e.g., over the metacarpophalangeal joint), the percept was considered within the location where the majority of the sensation occurred; however, if the size of the percept spread beyond the border then the percept was not considered stable. The first stimulation session (post-implantation day 6; Subject 2-U) resulted in an incomplete mapping of the array where maximum stimulation was not delivered to all 96 electrodes. The last two sessions (post-implantation days 26 and 27; Subject 2-U) were mapped using a different frequency (20 Hz). These three stimulation sessions were not included in the spatial stability analysis.

3. Results

The results presented here demonstrate that, using a 96 microelectrode array implanted into human peripheral nerves, up to 13 different movements could be decoded and a maximum of 86 percepts could be evoked.

3.1. Electrode impedances

For Subject 1-M, the mean *in vivo* impedance for working electrodes over the 29 day implant was 222 $\pm$ 133 kΩ (mean $\pm$ std, $n = 7$ sessions; figure 1(a)). Due to mechanical failure of the lead wires, the number of working electrodes dropped from 93 to 20 by the end of week 2, and then to 4 by the end of week 4. In Subject 2-U, the percutaneous connector was sutured to the skin to minimize strain applied to the wires, and no systematic failures indicating wire breakages occurred. The mean impedances for the working electrodes over the 31 day implant for this subject was 143 $\pm$ 76 kΩ (mean $\pm$ std, $n = 13$ sessions; figure 1(b)), and the number of working electrodes was 87 $\pm$ 5 (mean $\pm$ std). Impedances were found to vary significantly over the course of the study ($p < 0.0001$, Kruskal–Wallis test, Subject 2-U), with an increase from post-implantation days 3–10.

3.2. Recording and decoding of motor intent with high-count electrode arrays

Neural recordings were made while the subjects were asked to make volitional flexion, extension or abduction movements of their phantom fingers throughout the study period. Examples of action potentials recorded from the same electrodes over time are shown in figures 1(c) and (d) for each subject. In Subject 1-M, an average of 7 $\pm$ 9 electrodes recorded action potentials for the 6 recording sessions with a maximum of 20 electrodes recording action potentials on post-implantation day 3 (figure 1(e)). In Subject 2-U, an average of 22 $\pm$ 7 electrodes recorded action potentials for the 13 recording sessions with a maximum of 40 electrodes recording action potentials on post-implantation day 7 (figure 1(f)). The mean SNR of the action potentials recorded during all sessions for each subject were 5.2 $\pm$ 2.3 for Subject 1-M and 5.1 $\pm$ 2.8 for Subject 2-U (figures 1(e) and (f)). For Subject 2-U, after post-implantation day 10, there was no significant change in the SNR of the action potentials for the remainder of the study ($p = 0.24$, Kruskal–Wallis test).

3.2.1. Recording neural activity during different intended phantom finger movements. Subjects were cued to make different finger movements either by a computer cursor or by movement of virtual robotic fingers. The intent to flex or extend individual phantom digits produced spatiotemporal neural firing patterns that were visible in the high-pass filtered recording data (figures 2(a) and (b)). The patterns of neural activity varied across electrodes and movement types. Some electrodes recorded action potentials that were correlated with a single movement type (figure 2(a), middle finger flexion (MF), electrode 44, Subject 1-M) or movement of a single digit (figure 2(b), thumb, electrode 88, Subject 2-U); however, other electrodes recorded action potentials that correlated with multiple different fingers and movement types (figure 2(b), electrodes 13 and 44).

3.2.2. Multiple movements could be decoded offline. Estimated finger positions showed high correlations ($r = 0.9$) with the instruction variables for the best two movements (IF and MF) achieved in Subject 1-M and the best four movements (TF, IAb, IE, TE) achieved in Subject 2-U (figures 2(c) and (d)). Prediction accuracy decreased as the number of movements being estimated increased, with a value of $r = 0.48$ at 13 different finger movements for Subject 2-U (figure 2(f)). To validate the decode results, the electrode order was randomly shuffled between the training

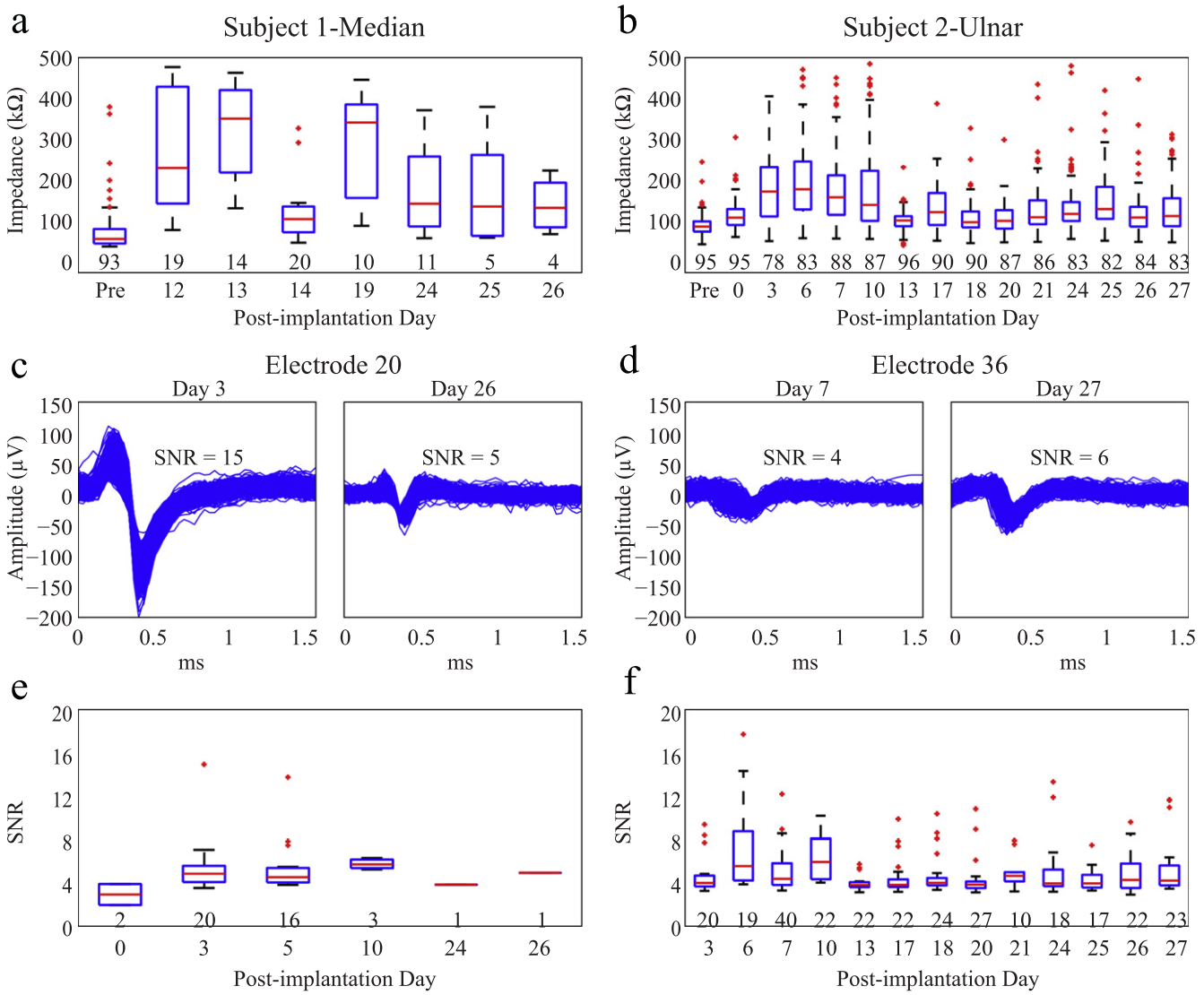

Figure 1. Electrode impedances and action potential recording quality. The left column of panels (a), (c), and (e) show data from Subject 1-M; and the right column of panels (b), (d), and (f) show data from Subject 2-U. (a) and (b) Box-and-whisker plots of impedances taken pre-implantation in saline and post-implantation throughout the study. The number below each boxplot is the number of working electrodes. (c) and (d) Action potentials recorded on example electrodes at two time points, one early and one late in the study, from each subject. (e) and (f) Box-and-whisker plots of signal-to-noise for all action potentials recorded on all electrodes throughout the study. The number below each boxplot is the number of electrodes that recorded action potentials during the individual experimental session.

and testing sets, and the firing rate data was decoded again. Using this shuffled data, the prediction accuracy dropped to $r = 0.14$ for 13 different movements (Subject 2-U). For Subject 2-U, the median decode performance for seven sessions spanning 23 days for the same eight movements was $r = 0.62 \pm 0.07$ (the 5 finger extension movements were added on post-implantation day 13 and were not included in this analysis).

3.2.3. Multiple movements could be decoded online. Data recorded from the median nerve was decoded online for middle and index phantom finger flexion, and the subject was able to move the graphical indicator to targets specific to each finger individually with a median time to trial completion of 9 ± 6 s (16 trials, 5 electrodes; figure 2(g)). Data recorded from the ulnar nerve was decoded online for thumb and little phantom finger flexions, and the subject was able to independently and proportionally control each of the virtual robotic fingers with a median time to trial completion of 2 ± 5 s (79 trials, 4 electrodes; figure 2(h)) (supplemental video 2). In each subject, online decodes were successful in providing simultaneous control of two graphical indicators (Subject 1-M) or two virtual prosthetic fingers (Subject 2-U) from the neural signals generate by movement of their phantom fingers. However, some crosstalk existed between these DOF, making independent control more difficult.

3.3. Intrafascicular microstimulation evoked sensory percepts

In Subject 1-M, single electrode stimulation on 17 electrodes over the course of the study evoked sensory percepts with an average threshold of 27 ± 20 μA (mean $\pm$ std) (figure 3(a))

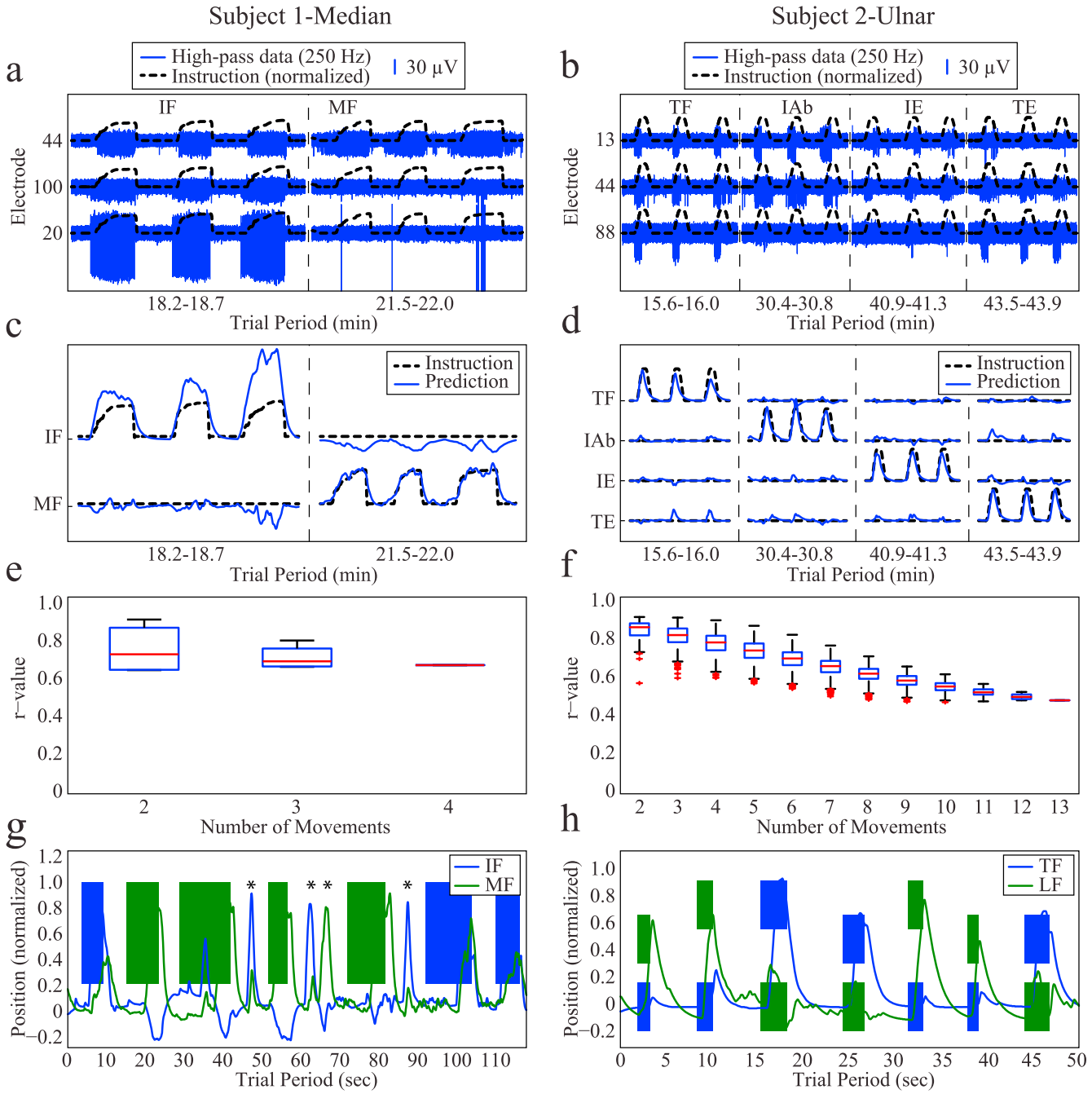

Figure 2. Decoding volitional phantom finger movements from peripheral nerve action potentials. The left column of panels (a), (c), (e), and (g) show data from Subject 1-M; and the right column of panels (b), (d), (f), and (h) show data from Subject 2-U. (a) and (b) High-pass filtered neural recordings (solid blue) made by three electrodes during phantom finger movements for Subject 1-M (post-implantation day 3) and Subject 2-U (post-implantation day 24). Superimposed is the instructed finger movement (dashed black). Action potentials can be seen in the high-pass filtered data extending out of the noise during the instruction period. (c) and (d) Kalman filter predictions for the best two movements for Subject 1-M and the best four movements for Subject 2-U. Only a subset of trials is shown. Prediction correlations of 0.9 were achieved using multi-unit firing rates calculated from unsorted spike events on 18 electrodes (Subject 1-M, post-implantation day 3) and 55 electrodes (Subject 2-U, post-implantation day 24). (e) and (f) Box-and-whisker plots of offline Kalman filter performance for all combinations of available movements using the same electrodes as in (c) and (d). (g) and (h) Examples of Kalman filter performance during online decode sessions for each subject. Boxes represent trial-by-trial target locations and the traces represent the Kalman filter predictions for the intended finger movement. To successfully complete a trial, the predicted finger movement must enter and remain in the target box for a specified hold duration (3000 (g) and 300 (h) ms). Asterisks highlight verbally-stated volitional movements made by the subject in the absence of a target.

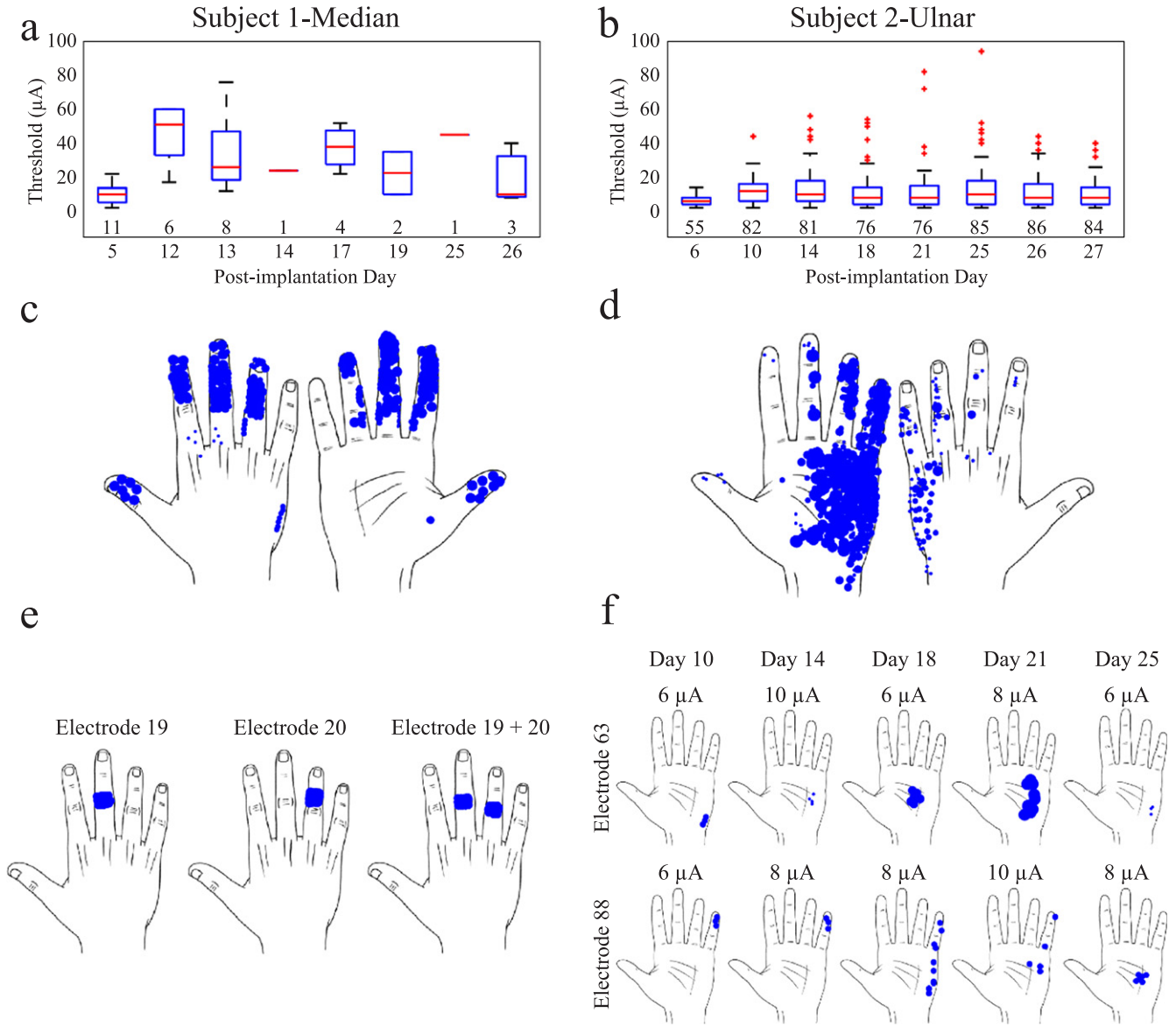

Figure 3. Electrical stimulation can evoke spatially distinct and stable sensory percepts. The left column of panels (a), (c) and (e) show data from Subject 1-M; and the right panels (b), (d), and (f) show data from Subject 2-U. (a) and (b) Sensory percept thresholds over the duration of the experimental period for both subjects. For subject 1-M, only a subset of electrodes was stimulated each session. For subject 2-U, except on post-implantation day 6, all 96 electrodes were stimulated each session. The number below each boxplot is the number of electrodes that evoked a sensory percept. (c) and (d) Results from intrafascicular stimulation of human median and ulnar nerves show evoked sensations in the phantom hand that approximately followed the expected spatial distributions for each nerve. The cumulative data from all microstimulation sessions is shown. (e) Single electrode stimulation (electrode 19 at 47 μA; electrode 20 at 15 μA) produced discrete sensory percepts, and when the same electrodes were stimulated simultaneously the two discrete percepts could be perceived simultaneously (Subject 1-M). The inter-electrode distance in this example was 400 μm. (f) Examples of percepts that were evoked by two different electrodes with one percept that was considered stable across all five sessions (electrode 63; top row of hands) and another that was stable for two consecutive sessions (electrode 88; bottom row of hands). Marked locations were felt simultaneously (Subject 2-U).

that were approximately located in an expected median nerve distribution (figure 3(c)). In Subject 2-U, when all 96 electrodes were stimulated individually, an average of 81 electrodes evoked sensory percepts with a mean threshold of 12 ± 11 μA (mean $\pm$ std) (figure 3(b)) that were approximately located in an expected ulnar nerve distribution (figure 3(d)). For this subject, no significant changes in the thresholds occurred after post-implantation day 10 ($p = 0.46$, Kruskal–Wallis test). Further, a comparison of all 96 electrodes demonstrated that the mean percept threshold for an electrode over the duration of the study (8 stimulation sessions) was negatively correlated ($r = -0.46$, $p < 0.0001$) with the number of days that an electrode recorded an action potential (13 recording sessions) (figures 4(a) and (b)).

3.3.1. Detection of multiple percepts simultaneously (Subject 1-M). For Subject 1-M, blind trial data was collected during three different experimental sessions on post-implantation days 13, 19, and 26 that included stimulation delivered via

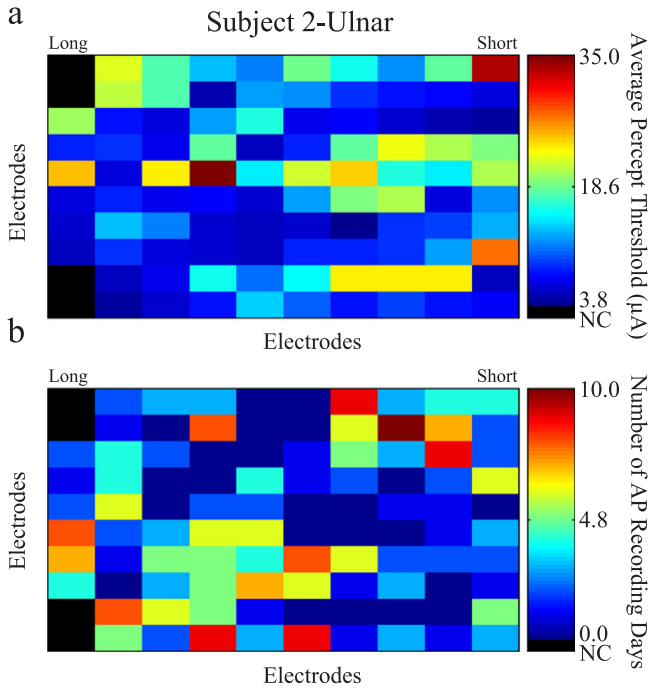

Figure 4. Spatial distributions of percept thresholds and action potential recordings for all 96 electrodes over 30 days. (a) Mean threshold needed to evoke a sensory percept via stimulation on each individual electrode over the duration of the study (8 total stimulation sessions, last stimulation session on day 27 post-implantation). (b) Number of days that each electrode recorded at an action potential over the duration of the study (13 total recording sessions, last session on day 27 post-implantation).

one electrode, a different electrode, both electrodes, or no electrodes. The following electrode-pair combinations were chosen to include varying inter-electrode distances using supra-threshold stimulation amplitudes: day 13—electrodes 16 (19 μA) and 19 (25 μA) with a 1200 μm distance; day 19—electrodes 19 (47 μA) and 20 (18 μA) at 400 μm distance; day 26—electrodes 20 (18 μA) and 46 (10 μA) at 1442 μm distance. Subject 1-M correctly discriminated between any-stimulation (stimulation on either electrode individually or both electrodes simultaneously) versus no-stimulation with 98% accuracy (58/59 total trials; day 13—19/19 trials; day 19—20/20 trails; day 26—19/20 trials). Subject 1-M correctly discriminated between spatially distinct percepts evoked by microstimulation delivered via one of two electrodes ($n = 5$ for each electrode per session) with 87% accuracy (26/30 total trials; day 13—9/10 trials; day 19—8/10 trials; day 26—9/10 trials). Spatial discrimination was accurately reported with electrodes separated by 400 μm (day 19) (figure 3(e)). Subject 1-M was also able to discriminate between simple patterns of stimulation, i.e., stimulation via either electrode individually versus simultaneous stimulation via both electrodes, with 84% accuracy (38/45 total trials; day 13—11/14 trials; day 19—13/15 trials; and day 26—14/16 trials).

3.3.2. Frequency and duration of stimulation modulated the quality of percepts (*Subject 1-M*). Subject 1-M was allowed to self-modulate the stimulation frequency from 1 to 100 Hz by pushing down on the manipulandum pressure sensor with the subject's intact hand with stimulation being delivered to a single electrode at 30 μA (post-implantation day 14). High frequencies (100–320 Hz) evoked an 'electric shock' like quality, and lower frequencies (1–25 Hz) and longer stimulation times (up to 60 s) could evoke more physiological percepts (e.g., pressure).

3.3.3. Location stability of percepts for all 96 electrodes over time (*Subject 2-U*). Five of the total eight stimulation sessions (post-implantation days 10–25) resulted in a complete mapping of all 96 electrodes at fixed parameters of 200 Hz, 0.2 ms durations, 200 μs pulse widths, and amplitudes that varied from 1 to 100 μA. Figure 3(f) shows examples of percepts evoked by two different electrodes over these five sessions. One of the electrodes (electrode 63) evoked a stable percept across all five sessions. The other electrode (electrode 88) was stable for two consecutive sessions. A total of 61 electrodes evoked percepts across all five sessions. Out of these 61 electrodes, 18 electrodes produced percepts that were considered stable within a defined region (see methods 2.6) of the phantom hand for two consecutive sessions (separated by 1–3 days). A total of eight electrodes evoked stable percepts for three consecutive sessions, four electrodes evoked stable percepts for four consecutive sessions, and three electrodes evoked stable percepts across all five stimulation sessions.

3.3.4. Number and quality of percepts for all 96 electrodes (*Subject 2-U*). The quality of evoked percepts in Subject 2-U combined across all five complete mapping sessions at 200 Hz included: 76 'tingle' percepts; 7 'pressure' percepts; and 216 'vibration' percepts. For the last two stimulation sessions, separated by one day, where the array was mapped at 20 Hz, a total of 76 electrodes evoked percepts on both days, with 17 electrodes evoking stable percepts. The percept quality evoked during these sessions included: 21 'tingle' percepts; 19 'pressure' or 'hair brush' percepts; 17 'vibration' percepts; and 96 'cold' or 'air brush' percepts. The subject noted that the 'tingle' and 'vibration' percepts evoked during each session were of a 'painful' quality.

3.4. Phantom limb sensations occurred post-stimulation in both subjects

Both subjects differentiated between phantom limb sensations (the normal feelings from their phantom hand) and phantom limb pains (percepts that were considered uncomfortable). Subjects reported an increase in the occurrence of phantom limb sensations that took on the characteristics of the sensory percepts evoked by electrical stimulation. At times, the post-stimulation sensations included percepts such as 'pressure' or 'hair brushing on the skin'. At other times, the subjects reported an increased occurrence of post-stimulation evoked phantom limb sensations that were painful, and the quality of such percepts included: 'electric shock,' 'stinging,' or 'tingling'. For each subject, percepts (duration $\approx$ 1–2 s) began

after the first day of stimulation, and had peak occurrences of $10\,h^{-1}$ for subject 1-M and $2–9\,h^{-1}$ for Subject 2-U. By 30 days post-explantation of the electrode array, both subjects no longer reported phantom sensations that were of the quality of stimulation-evoked percepts.

4. Discussion

In 2003, a human volunteer had a Utah microelectrode array (with all electrodes of the same length) implanted in his median nerve for 96 days. Although this study provided new data for the field of peripheral nerve interfaces, it also had several limitations including the following: stimulation and recording were carried out through 20 electrodes (out of the 100 electrodes that were implanted); no action potential data were presented to support that the devices were implanted intraneurally; no longitudinal data was presented to show the stability of the device capabilities (stimulating percepts and recording neural activity); and finally, decoding multiple DOF was not investigated [53, 68]. Here, we extended that work by investigating multiple aspects important for developing future bidirectional neural prostheses based on high-count microelectrode arrays, including: the quality of percepts evoked by microelectrode stimulation, frequency modulation of percept quality, the number of different movements that can be decoded using action potential data, and the overall recording and stimulation capabilities of microelectrode array devices over a 30 day period.

4.1. Stability of USEAs implanted for 30 days and potential for longer duration implants

In Subject 1-M, the impedances for the majority of the electrodes went out of specification at the end of the first week due to lead wire breakage; however, four electrodes remained viable for the duration of the implant. Suturing the percutaneous connector to the skin appeared to have reduced the chance of wire breakage in Subject 2-U (no observed wire breakages). The SNR was stable after day ten of implantation for Subject 2-U, and we hypothesize this may be due to the stabilization in the surrounding tissue as the acute inflammatory response begins to resolve [69]. Impedances varied significantly over the duration of the study with an increase during post-implantation days 3–10. This variability may reflect either changes in the electrode itself (surface chemistry of the iridium oxide) or changes in the electrode–tissue interface (cellular milieu). Furthermore, impedances may stabilize after 30 days as shown in previous studies of USEAs implanted in the feline sciatic nerve [70].

A robust percutaneous connector or a telemetry system will be needed before applications using microelectrode arrays achieve clinical utility. Also, the generation of microelectrode arrays used in this study have maximum electrode shank lengths of 1.5 mm, which limits the cross-sectional access to the deeper regions of the relatively large human peripheral nerves that are greater than 3 mm in diameter. Longer electrodes and/or multiple arrays may be needed to expand electrophysiological access across the entire diameter of the nerves.

A more robust containment system, an anchoring system, or a more compliant microelectrode array design may be required to achieve the very long functional lifetimes necessary for clinical applications. The tissue response to indwelling intrafascicular electrodes has shown that, although implantation of intraneural electrodes results in tissue damage, viable neurons are found within distances ($<150\,\mu m$) needed for safe stimulation of and selective recording from neurons after >30 days of implantation [70–72]. Additionally, Utah microelectrode arrays have been implanted for >5 year durations in motor cortex and continue to record neural signals that can be used to control external devices, suggesting the viability of this type of interface for longer duration implant times [10]. Both subjects were given dexamethasone and minocycline doses in order to potentially increase the quality of action potential recordings over time [58, 59]. However, additional control studies are needed to investigate whether administration of these drugs can improve neural signal longevity over long-term electrode array implantations.

In this study, action potentials were recorded across multiple microelectrodes for the duration of the 30 day implant, which validates that the devices remained intrafascicularly implanted for the duration of the study. Moreover, electrodes that reliably recorded action potentials throughout the study generally evoked percepts at lower stimulation amplitudes, suggesting that these electrodes were intrafascicularly implanted, while other electrodes that did not record action potentials may have been implanted between fascicles.

4.2. Neural recordings and decoding independent and proportional phantom finger movements

An important aspect of any decoded signal for controlling a prosthetic hand is that it can mediate proportional control. This was investigated in two ways. First, we used a linear Kalman Filter to decode the neural data, which provided a continuous estimate of finger position that was proportional to some linear combination of the neural signals. Second, we placed targets at various positions located between full extension and full flexion. This required that the subjects proportionally modulate the neural signals in order to acquire the targets and complete the task. The advantage of using a virtual prosthetic hand as opposed to an actual robotic hand was programmatic control of target size and distance. With a virtual hand, we were better able to quantify the accuracy and timing of neurally-controlled movements. For both subjects, the decoded neural activity patterns provided proportional control of finger position and, importantly, such control was achieved during the first recording session with each subject. Some crosstalk existed between the DOF, which sometimes made it difficult for the subjects to independently control different digits during the online experimentation.

The relationship between the central representation of motor control and the kinematics of movement is complex,

with activity in single neural units correlated with the movements of multiple finger muscles [73, 74]. The central and peripheral nervous systems control the synergistic biomechanics of the human hand [75]; however, current high-DOF prosthetic hands do not implement mechanical synergies [47, 48]. These synergies require co-activation of multiple muscles innervated by multiple nerves. The relationship between neural encoding and the hand biomechanics is further complicated by the possibility of post-amputation neural plasticity and the specific location of the array implantation along the proximal–distal nerve axis. Future work is needed to develop efficient mapping of these synergistic neural signals onto the non-synergistic mechanics of high-DOF prosthetic hands, or to develop prosthetic hands that accurately model the biomechanics of the human hand.

In this study we correlated finger positions of the subjects' phantom hand with the neural signals recorded in peripheral nerves, but did not study the influence of load/force or arm/hand posture on these efferent neural signals. There are complex neural systems throughout the hierarchy of sensory-motor control that will modulate the efferent neural signals in the peripheral nerve under different loads. For example, objects of different weights or movements with inertial dynamics will require dynamic grip forces even under isometric conditions. Further, different postures of the hand and arm will interact with movement dynamics and require differential modulation of the efferent neural signals for similar finger positions. Any decoding of neural signals must account for these complexities in order to provide naturalistic control of a high-DOF prosthetic hand. The development of algorithms that decode neural signals from peripheral nerves for prosthetic control will continue to an area of active research. Improving the performance of prosthetic hands will likely necessitate the incorporation of afferent sensory information, as well as efferent motor control signals, as inputs to decoding algorithms.

4.3. Stimulation-evoked sensory percepts

We explored the ability to evoke sensory percepts by injecting currents into the peripheral nerves via many of the electrodes in the implanted arrays. In both subjects spatially discrete somatosensory percepts were evoked using low levels of current. These spatially discrete percepts could be used for registering contact of the fingers in a prosthetic hand with an object with high spatial fidelity. Translations of non-physiological percepts into more physiological percepts was achieved by varying the frequency and the duration of microstimulation, i.e., the percept changed from an 'electric shock-like tingle' to pressure, indicating that modulation of microstimulation parameters may be used to address submodalities of somatosensation. Subject 1-M was able to detect and discriminate simple patterns of microstimulation, suggesting the more complex spatio-temporal patterns of stimulation could provide more complex sensation such as brushing or sliding across the skin. Subject 1-M noted:

(1) 'As I am pressing that down there (on the manipulandum pressure sensor) on that intensity and moving the finger a little bit…this (the sensory percept) stayed on that finger as I was moving it'.
(2) 'As they speed up (the stimulation frequency increasing from 1 to 100 Hz) I can feel more of the finger. … It applies pressure on the index and this finger (of the phantom hand, indicated by pointing to the tip of the ring finger on the subject's intact hand)'.
(3) Question from the experimenter: 'Could you use this stimulation to recreate touch'?

Answer from Subject 1-M: 'Definitely…The more you press it (subject pressed on manipulandum pressure sensor changing the frequency from 1 to 100 Hz) you can sense it (the phantom finger) more. … And you'll get the sense of touch, 'cause that's what you did for me'.

This subject was also very accurate at reporting the absence of any sensation when no microstimulation was provided. The stability of the stimulation-evoked percepts was assessed, and indicated that while evoked percepts were grossly stable they did change over time. The changes in evoked percepts likely results from micro-motion of the electrode array relative to the nerve, and perceptual stability could be increased by improving the systems used to contain the array and anchor it to the nerve. The results presented here indicated that implantations of microelectrode arrays into the peripheral nerves of amputees could provide sensory feedback that would improve the manipulation of objects using highly dexterous prosthetic hands.

Future studies are warranted to investigate the stimulation parameters that evoke other sensations, such as proprioception, as well as, long-duration stimulation to evoke long-lasting sensations. Recent studies have shown modulation of stimulation intensity with a time-variant pulse width results in more natural evoked perceptions [45] and employing these methods may improve the quality of percepts produced by microelectrodes. Moreover, Tan *et al* have also demonstrated stability of percept location may stabilize after 27 weeks post implantation[56], and thus, longer duration USEA studies are warranted to assess such time periods.

4.4. Post-stimulation evoked sensory percepts

The subjects experienced post-stimulation percepts that occasionally had the uncomfortable or painful qualities of the percepts evoked by some electrical stimulation. Importantly, neither of the subjects experienced these qualities of percepts prior to participating in the study. Future work should address optimizing microstimulation parameters to produce only physiologically relevant sensory percepts, and investigate plasticity in the central motor and sensory neural representations resulting from long-term microstimulation of the peripheral nerves [76–80]. Subject 2-U noted the feeling of the non-painful post-stimulation percepts in the subject's phantom limb sensation diary:

> 'I have had the kind of fluttering or breath-on-the-skin or hair-pressure that I had often in the

> lab session today. (Located in the web area between my PIF (phantom index finger) and PMF (phantom middle finger).) It is as if now that the sensation has been awakened, it keeps registering, regardless of context—a little like a kid using a new vocabulary word liberally or a cook using a favourite spice or herb in all kinds of meals…'

These 'awakened' phantom limb sensations may have implications for embodiment of neural prostheses. Consistent stimulation of the nerve may engage or reactivate central neural circuits that encode the representation of the phantom or prosthetic limb. This embodiment of a prosthetic limb could be enhanced by coupling the nerve stimulation with simultaneous input from other sensory modalities, e.g. vision of the limb being touch.

5. Conclusion

Numerous electrodes on the arrays recorded neural activity patterns from residual nerves that were volitionally generated by the intention to flex, extend or abduct individual digits in the subjects' missing hand. Up to thirteen movement types could be decoded offline, and proportional control of up to two digits of a virtual prosthesis was achieved online. Stimulation of up to 96 electrodes, either one-at-a-time or via small groups simultaneously, evoked multiple percepts that were spatially distributed across the phantom hands in anatomically appropriate distributions. The relatively large number of channels of motor and sensory information provided by the microelectrode arrays indicate that such arrays can serve as a neural interface for controlling high-DOF prosthetic limbs. The subtle verbal descriptions of evoked perceptions from the subjects indicated an attempt to integrate the sensations, either cognitively or perhaps due to neural plasticity, into their subjective bodily representation. Patients outfitted with a highly dexterous prosthetic limb controlled through such a bi-directional peripheral nerve interface might begin to think of the prosthesis not as a piece of hardware attached to their arm, but rather, as an integral extension of themselves.

Acknowledgments

Research reported in this publication was sponsored by (1) National Institutes of Health (NIH), National Center for Advancing Translational Sciences (NCATS), Award 1ULTR001067 and (2) the Defence Advanced Research Projects Agency (DARPA), Microsystems Technology Office (MTO), under the auspices of Dr Jack Judy through the Space and Naval Warfare Systems Center, Pacific Grant/Contract No. N66001-12-C-4042. The authors wish to thank the staff at their respective hospitals for their assistance in conducting this study, and most importantly the patients who selflessly participated in this research.

References

[1] Carmena J M, Lebedev M A, Crist R E, O'Doherty J E, Santucci D M, Dimitrov D F, Patil P G, Henriquez C S and Nicolelis M A 2003 Learning to control a brain–machine interface for reaching and grasping by primates *PloS Biol.* **1** E42

[2] Kemere C, Santhanam G, Yu B M, Afshar A, Ryu S I, Meng T H and Shenoy K V 2008 Detecting neural-state transitions using hidden Markov models for motor cortical prostheses *J. Neurophysiol.* **100** 2441–52

[3] Musallam S, Corneil B D, Greger B, Scherberger H and Andersen R A 2004 Cognitive control signals for neural prosthetics *Science* **305** 258–62

[4] Suner S, Fellows M R, Vargas-Irwin C, Nakata G K and Donoghue J P 2005 Reliability of signals from a chronically implanted, silicon-based electrode array in non-human primate primary motor cortex *IEEE Trans. Neural Syst. Rehabil. Eng.* **13** 524–41

[5] Sussillo D, Nuyujukian P, Fan J M, Kao J C, Stavisky S D, Ryu S and Shenoy K 2012 A recurrent neural network for closed-loop intracortical brain–machine interface decoders *J. Neural Eng.* **9** 026027

[6] Velliste M, Perel S, Spalding M C, Whitford A S and Schwartz A B 2008 Cortical control of a prosthetic arm for self-feeding *Nature* **453** 1098–101

[7] Aflalo T *et al* 2015 Neurophysiology decoding motor imagery from the posterior parietal cortex of a tetraplegic human *Science* **348** 906–10

[8] Collinger J L, Wodlinger B, Downey J E, Wang W, Tyler-Kabara E C, Weber D J, McMorland A J, Velliste M, Boninger M L and Schwartz A B 2013 High-performance neuroprosthetic control by an individual with tetraplegia *Lancet* **381** 557–64

[9] Gilja V *et al* 2015 Clinical translation of a high-performance neural prosthesis *Nat. Med.* **21** 1142–5

[10] Hochberg L R *et al* 2012 Reach and grasp by people with tetraplegia using a neurally controlled robotic arm *Nature* **485** 372–5

[11] Hochberg L R, Serruya M D, Friehs G M, Mukand J A, Saleh M, Caplan A H, Branner A, Chen D, Penn R D and Donoghue J P 2006 Neuronal ensemble control of prosthetic devices by a human with tetraplegia *Nature* **442** 164–71

[12] Jarosiewicz B *et al* 2015 Virtual typing by people with tetraplegia using a self-calibrating intracortical brain–computer interface *Sci. Transl. Med.* **7** 313ra179

[13] Kim S P, Simeral J D, Hochberg L R, Donoghue J P, Friehs G M and Black M J 2011 Point-and-click cursor control with an intracortical neural interface system by humans with tetraplegia *IEEE Trans. Neural Syst. Rehabil. Eng.* **19** 193–203

[14] Klaes C *et al* 2015 Hand shape representations in the human posterior parietal cortex *J. Neurosci.* **35** 15466–76

[15] Simeral J D, Kim S-P, Black M J, Donoghue J P and Hochberg L R 2011 Neural control of cursor trajectory and click by a human with tetraplegia 1000 days after implantation of an intracortical microelectrode array *J. Neural Eng.* **8** 025027

[16] Wodlinger B, Downey J E, Tyler-Kabara E C, Schwartz A B, Boninger M L and Collinger J L 2015 Ten-dimensional anthropomorphic arm control in a human brain–machine interface: difficulties, solutions, and limitations *J. Neural Eng.* **12** 016011

[17] Anderson N R, Blakely T, Schalk G, Leuthardt E C and Moran D W 2012 Electrocorticographic (ECoG) correlates of human arm movements *Exp. Brain Res.* **223** 1–10

[18] Chestek C A, Gilja V, Blabe C H, Foster B L, Shenoy K V, Parvizi J and Henderson J M 2013 Hand posture

classification using electrocorticography signals in the gamma band over human sensorimotor brain areas *J. Neural Eng.* **10** 026002
[19] Kellis S, Hanrahan S, Davis T, House P A, Brown R and Greger B 2012 Decoding hand trajectories from micro-electrocorticography in human patients *Annual Int. Conf. Proc. IEEE Engineering Medicine Biology Society (EMBC) 2012* pp 4091–4
[20] Kellis S, Miller K, Thomson K, Brown R, House P and Greger B 2010 Decoding spoken words using local field potentials recorded from the cortical surface *J. Neural Eng.* **7** 056007
[21] Kellis S S, House P A, Thomson K E, Brown R and Greger B 2009 Human neocortical electrical activity recorded on nonpenetrating microwire arrays: applicability for neuroprostheses *Neurosurg. Focus* **27** E9
[22] Leuthardt E C, Freudenberg Z, Bundy D and Roland J 2009 Microscale recording from human motor cortex: implications for minimally invasive electrocorticographic brain–computer interfaces *Neurosurg. Focus.* **27** E10
[23] Leuthardt E C, Gaona C, Sharma M, Szrama N, Roland J, Freudenberg Z, Solis J, Breshears J and Schalk G 2011 Using the electrocorticographic speech network to control a brain–computer interface in humans *J. Neural Eng.* **8** 036004
[24] Leuthardt E C, Pei X M, Breshears J, Gaona C, Sharma M, Freudenberg Z, Barbour D and Schalk G 2012 Temporal evolution of gamma activity in human cortex during an overt and covert word repetition task *Front. Hum. Neurosci.* **6** 99
[25] Leuthardt E C, Schalk G, Wolpaw J R, Ojemann J G and Moran D W 2004 A brain–computer interface using electrocorticographic signals in humans *J. Neural Eng.* **1** 63–71
[26] Pei X, Leuthardt E C, Gaona C M, Brunner P, Wolpaw J R and Schalk G 2011 Spatiotemporal dynamics of electrocorticographic high gamma activity during overt and covert word repetition *Neuroimage* **54** 2960–72
[27] Schalk G, Kubanek J, Miller K J, Anderson N R, Leuthardt E C, Ojemann J G, Limbrick D, Moran D, Gerhardt L A and Wolpaw J R 2007 Decoding two-dimensional movement trajectories using electrocorticographic signals in humans *J. Neural Eng.* **4** 264–75
[28] Schalk G and Leuthardt E C 2011 Brain–computer interfaces using electrocorticographic signals *IEEE Rev. Biomed. Eng.* **4** 140–54
[29] Schalk G, Miller K J, Anderson N R, Wilson J A, Smyth M D, Ojemann J G, Moran D W, Wolpaw J R and Leuthardt E C 2008 Two-dimensional movement control using electrocorticographic signals in humans *J. Neural Eng.* **5** 75–84
[30] Wang W *et al* 2013 An electrocorticographic brain interface in an individual with tetraplegia *PLoS One* **8** e55344
[31] Wang W *et al* 2009 Human motor cortical activity recorded with Micro-ECoG electrodes, during individual finger movements *Annual Int. Conf. Proc. IEEE Engineering Medicine Biology Society (EMBC) 2009* pp 586–9
[32] Hiremath S V *et al* 2015 Human Perception of Electrical Cortical Surface Stimulation at the Somatosensory Cortex *Neuroscience Meeting Planner* Program No. 428.07. 2015
[33] Darpa 2015 Neurotechnology Provides Near-Natural Sense of Touch - Revolutionizing Prosthetics program achieves goal of restoring sensation [press release]. http://www.darpa.mil/news-events/2015-09-11
[34] Hargrove L J, Simon A M, Young A J, Lipschutz R D, Finucane S B, Smith D G and Kuiken T A 2013 Robotic leg control with EMG decoding in an amputee with nerve transfers *New Engl. J. Med.* **369** 1237–42
[35] Kuiken T A, Li G, Lock B A, Lipschutz R D, Miller L A, Stubblefield K A and Englehart K B 2009 Targeted muscle reinnervation for real-time myoelectric control of multifunction artificial arms *JAMA* **301** 619–28
[36] Clark G A, Wendelken S, Page D M, Davis T, Wark H A C, Normann R A, Warren D J and Hutchinson D T 2014 Using multiple high-count electrode arrays in human median and ulnar nerves to restore sensorimotor function after previous transradial amputation of the hand *36th Annual Int. Conf. Proc. IEEE Engineering Medicine Biology Society (EMBC)* pp 1977–80
[37] Dhillon G S and Horch K W 2005 Direct neural sensory feedback and control of a prosthetic arm *IEEE Trans. Neural Syst. Rehabil. Eng.* **13** 468–72
[38] Dhillon G S, Lawrence S M, Hutchinson D T and Horch K W 2004 Residual function in peripheral nerve stumps of amputees: implications for neural control of artificial limbs *J. Hand Surg. Am.* **29** 605–15 discussion 616–8
[39] Garde K, Keefer E, Botterman B, Galvan P and Romero M I 2009 Early interfaced neural activity from chronic amputated nerves *Front. Neuroeng.* **2** 5
[40] Horch K, Meek S, Taylor T G and Hutchinson D T 2011 Object discrimination with an artificial hand using electrical stimulation of peripheral tactile and proprioceptive pathways with intrafascicular electrodes *IEEE Trans. Neural Syst. Rehabil. Eng.* **19** 483–9
[41] Polasek K H, Schiefer M A, Pinault G C, Triolo R J and Tyler D J 2009 Intraoperative evaluation of the spiral nerve cuff electrode on the femoral nerve trunk *J. Neural Eng.* **6** 066005
[42] Polasek K H, Hoyen H A, Keith M W and Tyler D J 2007 Human nerve stimulation thresholds and selectivity using a multi-contact nerve cuff electrode *IEEE Trans. Neural Syst. Rehabil. Eng.* **15** 76–82
[43] Raspopovic S *et al* 2014 Restoring natural sensory feedback in real-time bidirectional hand prostheses *Sci. Transl. Med.* **6** 222ra19
[44] Rossini P M *et al* 2010 Double nerve intraneural interface implant on a human amputee for robotic hand control *Clin. Neurophysiol.* **121** 777–83
[45] Tan D W, Schiefer M A, Keith M W, Anderson J R, Tyler J and Tyler D J 2014 A neural interface provides long-term stable natural touch perception *Sci. Transl. Med.* **6** 257ra138
[46] Zlotolow D A and Kozin S H 2012 Advances in upper extremity prosthetics *Hand Clin.* **28** 587–93
[47] Burck J M, Bigelow J D and Harshbarger S D 2011 Revolutionizing prosthetics: systems engineering challenges and opportunities *Johns Hopkins APL Tech. Dig.* **30** 186–97
[48] Resnik L, Klinger S L and Etter K 2014 The DEKA Arm: its features, functionality, and evolution during the veterans affairs study to optimize the DEKA Arm *Prosthet. Orthot. Int.* **38** 492–504
[49] Schultz A E, Marasco P D and Kuiken T A 2009 Vibrotactile detection thresholds for chest skin of amputees following targeted reinnervation surgery *Brain Res.* **1251** 121–9
[50] Schiefer M A, Polasek K H, Triolo R J, Pinault G C and Tyler D J 2010 Selective stimulation of the human femoral nerve with a flat interface nerve electrode *J. Neural Eng.* **7** 26006
[51] Boretius T, Badia J, Pascual-Font A, Schuettler M, Navarro X, Yoshida K and Stieglitz T 2010 A transverse intrafascicular multichannel electrode (TIME) to interface with the peripheral nerve *Biosens. Bioelectron.* **26** 62–9
[52] Branner A, Stein R B and Normann R A 2001 Selective stimulation of cat sciatic nerve using an array of varying-length microelectrodes *J. Neurophysiol.* **85** 1585–94
[53] Gasson M, Hutt B, Goodhew I, Kyberd P and Warwick K 2005 Invasive neural prosthesis for neural signal detection and

nerve stimulation *Int. J. Adapt. Control Signal Process.* **19** 365–75
[54] Yoshida K and Horch K 1993 Selective stimulation of peripheral nerve fibers using dual intrafascicular electrodes *IEEE Trans. Biomed. Eng.* **40** 492–4
[55] Jia X, Koenig M A, Zhang X, Zhang J, Chen T and Chen Z 2007 Residual motor signal in long-term human severed peripheral nerves and feasibility of neural signal-controlled artificial limb *J. Hand Surg. Am.* **32** 657–66
[56] Tan D W, Schiefer M A, Keith M W, Andersen R A and Tyler D J 2015 Stability and selectiviey of a chronic, multi-contact cuff electrode for sensory stimulation in human amputees *J. Neural Eng.* **12** 026002
[57] Ochoa J and Torebjork E 1989 Sensations evoked by intraneural microstimulation of C nociceptor fibres in human skin nerves *J. Physiol.* **415** 583–99
[58] Rennaker R L, Miller J, Tang H and Wilson D A 2007 Minocycline increases quality and longevity of chronic neural recordings *J. Neural Eng.* **4** L1–5
[59] Spataro L, Dilgen J, Retterer S, Spence A J, Isaacson M, Turner J N and Shain W 2005 Dexamethasone treatment reduces astroglia responses to inserted neuroprosthetic devices in rat neocortex *Exp. Neurol.* **194** 289–300
[60] Nordhausen C T, Maynard E M and Normann R A 1996 Single unit recording capabilities of a 100 microelectrode array *Brain Res.* **726** 129–40
[61] Wu W, Gao Y, Bienenstock E, Donoghue J P and Black M J 2006 Bayesian population decoding of motor cortical activity using a Kalman filter *Neural Comput.* **18** 80–118
[62] Davoodi R and Loeb G E 2012 Real-time animation software for customized training to use motor prosthetic systems *IEEE Trans. Neural Syst. Rehabil. Eng.* **20** 134–42
[63] Lilly J C, Hughes J R, Alvord E C Jr and Galkin T W 1955 Brief, noninjurious electric waveform for stimulation of the brain *Science* **121** 468–9
[64] McCreery D B, Agnew W F, Yuen T G and Bullara L 1990 Charge density and charge per phase as cofactors in neural injury induced by electrical stimulation *IEEE Trans. Biomed. Eng.* **37** 996–1001
[65] Cogan S F 2008 Neural stimulation and recording electrodes *Annu. Rev. Biomed. Eng.* **10** 275–309
[66] Davis T S, Parker R A, House P A, Bagley E, Wendelken S, Normann R A and Greger B 2012 Spatial and temporal characteristics of V1 microstimulation during chronic implantation of a microelectrode array in a behaving macaque *J. Neural Eng.* **9** 065003
[67] Troyk P R, Detlefsen D E, Cogan S F, Ehrlich J, Bak M, McCreery D B, Bullara L and Schmidt E 2004 'Safe' charge-injection waveforms for iridium oxide (AIROF) microelectrodes *IEMBS '04 24th Annual Int. Conf. Proc. IEEE Engineering Medicine Biology Society* pp 4141–4
[68] Warwick K, Gasson M, Hutt B, Goodhew I, Kyberd P, Andrews B, Teddy P and Shad A 2003 The application of implant technology for cybernetic systems *Arch. Neurol.* **60** 1369–73
[69] Anderson J M, Rodriguez A and Chang D T 2008 Foreign body reaction to biomaterials *Semin. Immunol.* **20** 86–100
[70] Branner A, Stein R B, Fernandez E, Aoyagi Y and Normann R A 2004 Long-term stimulation and recording with a penetrating microelectrode array in cat sciatic nerve *IEEE Trans. Biomed. Eng.* **51** 146–57
[71] Christensen M B, Pearce S M, Ledbetter N M, Warren D J, Clark G A and Tresco P A 2014 The foreign body response to the Utah Slant electrode array in the cat sciatic nerve *Acta Biomater.* **10** 4650–60
[72] Wark H A, Mathews K S, Normann R A and Fernandez E 2014 Behavioral and cellular consequences of high-electrode count Utah Arrays chronically implanted in rat sciatic nerve *J. Neural Eng.* **11** 046027
[73] Egan J, Baker J, House P A and Greger B 2012 Decoding dexterous finger movements in a neural prosthesis model approaching real-world conditions *IEEE Trans. Neural Syst. Rehabil. Eng.* **20** 836–44
[74] Schieber M H and Hibbard L S 1993 How somatotopic is the motor cortex hand area? *Science* **261** 489–92
[75] Poston B, Danna-Dos Santos A, Jesunathadas M, Hamm T M and Santello M 2010 Force-independent distribution of correlated neural inputs to hand muscles during three-digit grasping *J. Neurophysiol.* **104** 1141–54
[76] Allard T, Clark S A, Jenkins W M and Merzenich M M 1991 Reorganization of somatosensory area 3b representations in adult owl monkeys after digital syndactyly *J. Neurophysiol.* **66** 1048–58
[77] Kaas J H, Merzenich M M and Killackey H P 1983 The reorganization of somatosensory cortex following peripheral nerve damage in adult and developing mammals *Annu. Rev. Neurosci.* **6** 325–56
[78] Merzenich M M, Kaas J H, Wall J, Nelson R J, Sur M and Felleman D 1983 Topographic reorganization of somatosensory cortical areas 3b and 1 in adult monkeys following restricted deafferentation *Neuroscience* **8** 33–55
[79] Merzenich M M, Kaas J H, Wall J T, Sur M, Nelson R J and Felleman D J 1983 Progression of change following median nerve section in the cortical representation of the hand in areas 3b and 1 in adult owl and squirrel monkeys *Neuroscience* **10** 639–65
[80] Xerri C, Merzenich M M, Jenkins W and Santucci S 1999 Representational plasticity in cortical area 3b paralleling tactual-motor skill acquisition in adult monkeys *Cereb. Cortex* **9** 264–76